Figure 5. RIOKs drive proliferation and survival of GBM cells in a p53-dependent manner. (A) WST-1 assays. Following selection for shRNA expression, proliferation was measured with WST-1 reagent and quantified as the fold increase in absorbance between day 0 and day 3, normalized to controls treated with a nontargeting shRNA. 2 shRNAs tested per RIO kinase. P values refer to one-way ANOVA with Dunnett post test. Knockdown verified in Figure S13. (B) FACS analysis of cell cycle. Fixed cells were stained with propidium iodide for DNA content 72 hrs after siRNA transfection. Knockdown verified in Figure S13. (C, D) RIOK1 or RIOK2 knockdown stimulated apoptosis of neurosphere cultures, such as GBM39 and GBM301 (brightfield, D), evidenced by apoptotic features (D) and PARP cleavage, which indicates pro-apoptotic caspase activity ($PARP^{fl}$ indicates full-length PARP, $PARP^{cl}$ indicates cleaved PARP, in both long and short exposures). RIOK1 or RIOK2 knockdown did not significantly stimulate apoptosis in p53-mutant cells, such as GBM6, evidenced by lack of significant PARP cleavage. ΔEGFR-positive: GBM39, GBM301, and GBM6. PTEN-mutant: GBM301. PTEN-intact: GBM39 and GBM6. Cells harvested 96 hrs post-lentiviral infection. (E) Annexin V staining for apoptosis in U87MG cells, quantified by FACS. Controls (left) were treated with equivalent amounts of nontargeting control siRNAs alone (light blue) or control siRNAs mixed 1:1 with p53 siRNAs (dark blue). RIOK1 and RIOK2 siRNAs were mixed 1:1 with control (light blue) or p53 siRNAs (dark blue). Data is represented as the fold change in Annexin V-positive cells in the RIOK knockdown samples compared to corresponding control samples. Knockdown verified in Figure S13. (F) RIOK1 or RIOK2 knockdown upregulates p53 and p21 expression, which is blocked by concurrent RpL11 knockdown. For RpL11 experiments, cells were treated with equivalent amounts of siRNAs mixed 1:1 for control and experimental samples. Cells were harvested 72 hrs post-transfection.
doi:10.1371/journal.pgen.1003253.g005

dampen apoptosis and thus preserve signaling defects. Compared to controls, RIOK1 or RIOK2 knockdown led to reduced phosphorylation of Akt at Serine-473 and reduced phosphorylation of Akt target proteins such as FOXO3 (Figure 6C, Figure S17). This occurred in both p53 wild-type and p53 mutant GBM cells (Figure 6C, Figure S17). Serine-473 is phosphorylated by Tor complex 2, (TORC2) [46], and in yeast and human cancer cells, TORC2 phosphorylation of Akt is stimulated by mature ribosomes, which can bind to both TORC2 and Akt to mediate their interaction, and TORC2 activity is blocked by defects in ribosome biogenesis [60]. Given that RIOK1 and RIOK2 loss causes defects in 40S ribosome maturation [17,18,19], and that we discovered that RIOK1 and RIOK2 bind to TORC2 components, we hypothesized that RIOK1 and RIOK2 knockdown interferes with TORC2 activity. Consistent with this, other readouts of TORC2 activity, such as phosphorylation and levels of NDRG1 [60], were reduced (Figure 6C, Figure S17), demonstrating that TORC2 activity is downregulated by RIOK1 and RIOK2 loss. This is consistent with recent findings demonstrating a requirement for TORC2 signaling in Drosophila glial neoplasia as well as human GBM cells [9,48,49]. However, the effects of RIOK loss on Akt signaling were not limited to the TORC2-dependent substrates. Phosphorylation of other Akt substrates, such as PRAS40 and TSC2, can also be reduced upon RIO kinase knockdown (Figure 6C). Thus, RIOK1 and RIOK2 are necessary for Akt signaling in GBM cells. Over-all, our results strongly suggest that functional reduction of RIOK1 and RIOK2 results in loss of Akt activity and p53 activation to drive cell cycle arrest, chemosensitivity, and apoptosis in Akt-dependent GBM cells with intact p53 (Figure 7).

Discussion

From a *Drosophila* genetic screen, we identified genes encoding 16 novel kinases that affect EGFR- and PI3K- dependent neoplastic glial transformation. We found that a subset of human orthologs for these novel kinases, including RIOK1 and RIOK2, are subject to alterations in GBM. RIOK1 and RIOK2, two related and highly conserved atypical kinases, become upregulated in an Akt-dependent manner in GBM cells. Our results show that RIOK2 forms a complex with RIOK1 and TORC2 signaling components, drives activation of TORC2-dependent Akt signaling, and stimulates glial tumorigenesis. Furthermore, we found that, in GBM cells, RIOK1 or RIOK2 loss causes a reduction in Akt signaling towards TORC2-depdendent targets and provokes p53-dependent apoptosis, cell cycle exit, and chemosensitivity. Thus, our loss-of-function and gain-of-function data imply that RIOK2 creates a feedforward loop that promotes and maintains Akt activity, and disruption of this loop is sufficient to trigger chemosensitivity and apoptosis in Akt-dependent GBM cells with intact p53 (Figure 7). Our results may have broad relevance to other cancers since RIOK2 is strongly expressed in a range of other more common tumor types associated with high Akt activity, such as breast and prostate cancers (Figure S18). Further study of the RIO kinases as well as other kinases identified in our *Drosophila* screen may reveal new insights into the signaling defects underlying GBM and related cancers.

RIOK1 and RIOK2 upregulation was associated with Akt activity in both GBM tumor specimens and cultured cells, and our results show that Akt signaling regulates RIO kinase protein stability, although the exact mechanism by which Akt regulates RIO kinase levels remains undetermined. RIOK2 has several putative and mapped phosphorylation sites, including at least one putative Akt phosphorylation site (www.phosphosite.org, Figure S8). Other studies show that RIOK2 phosphorylation can be stimulated by EGFR, and can be carried out by Polo-like kinase 1 [21,61], and perhaps these events contribute to Akt-mediated regulation of RIO kinase levels. Of note, though standard GBM cells lacking PTEN showed high levels of RIO kinase expression, non-transformed astrocytes lacking PTEN did not show high levels of endogenous RIO kinase protein expression relative to astrocytes with intact PTEN. Therefore, other factors present in GBM cells must also contribute to elevated RIO kinase levels.

To date, published studies show that the RIO kinases act as ribosome assembly factors that transiently associate with the 40S subunit to promote ribosome maturation and translation initiation [17,18,20]. Given that mature ribosomes are required for TORC2 activation and Akt phosphorylation at Serine-473 [60], disruption of Akt signaling upon RIOK knockdown may be a result of defective ribosome biogenesis caused by RIO kinase loss. However, the RIO kinases may have a much more direct role in promoting and maintaining Akt activity given that RIOK2 binds to RIOK1 and to components of the TORC2 complex, which is consistent with recent studies in yeast showing that Rio2p can bind to Tor2 [22]. Given that Rio2p is released from mature ribosomes in a regulated process [20], it is possible that the reason mature ribosomes promote TORC2 signaling is because they release free cytoplasmic RIOK2 that then stimulates TORC2 assembly or activity. The specific interplay between the RIO kinases and mTor signaling, ribosome biogenesis, protein translation, and Akt signaling will require additional investigation in the context of both normal and abnormal PI3K and RTK signaling, and may involve other as yet undetermined factors.

Although RIOK1 and RIOK2 loss can cause defects in ribosome maturation [17,18], in GBM cells the effects of RIO loss are not generic and instead are genotype-specific: p53 null mutant GBM cells showed no major cell cycle defects or apoptosis upon loss of these kinases. This specificity is derived from p53 upregulation and activation induced by the RpL11 ribosomal protein in response to RIOK loss. In humans, activation of the

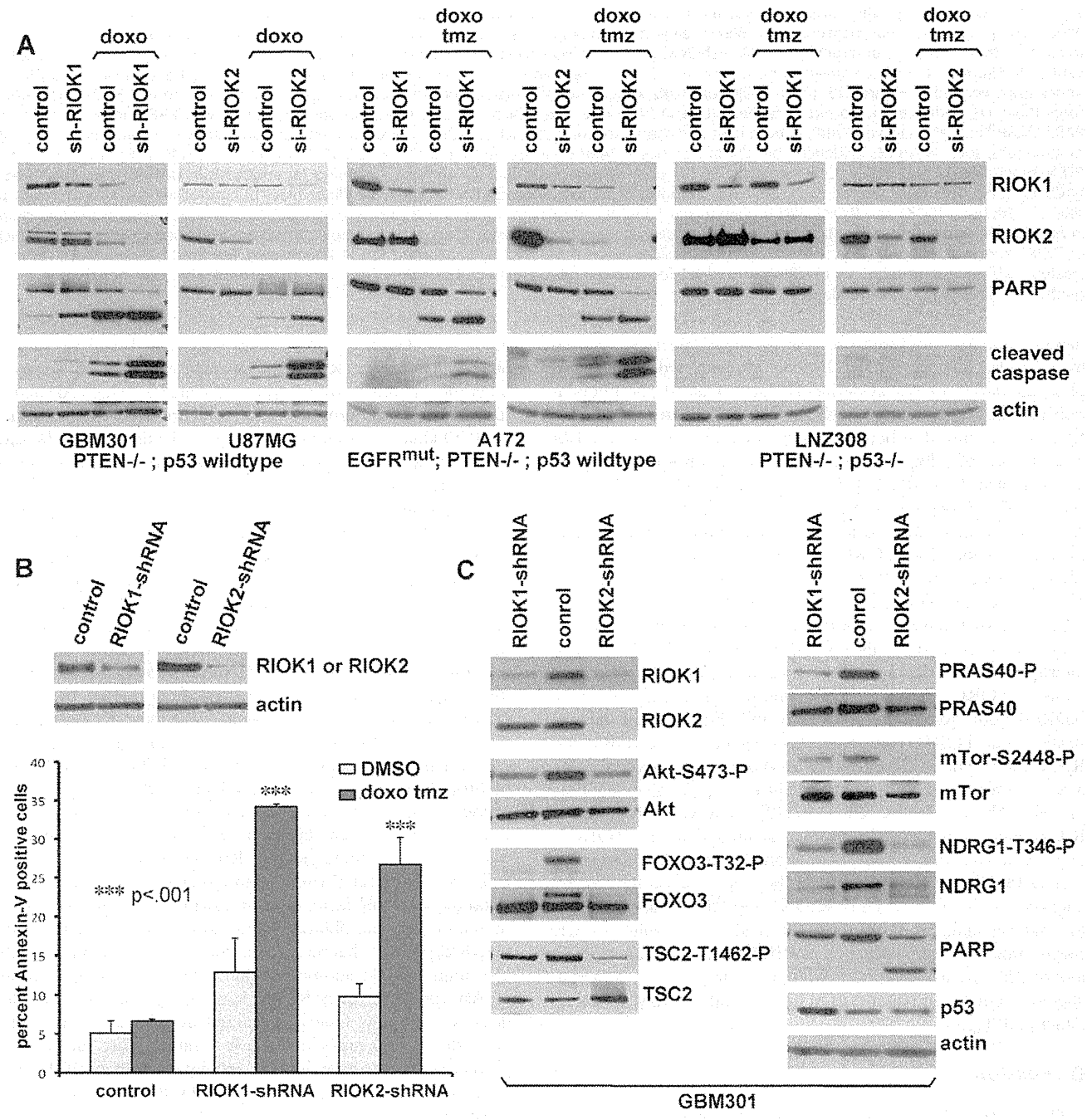

Figure 6. Loss of RIOK1 or RIOK2 function chemosensitizes GBM cells and reduces TORC2-Akt signaling. (A) Knockdown of RIOK1 or RIOK2 sensitizes GBM cells to apoptosis in response to treatment with doxorubicin (doxo) and temozolomide (tmz), as evidenced by blots for active caspase-3 and PARP cleavage (A). All samples blotted for RIOK1 and RIOK2 to confirm changes in RIOK1 levels with RIOK2 knockdown, evident in p53-wild-type GBM cell lines. The RIOKs also decline with doxorubicin treatment. GBM301 cells were treated for 24 hrs with 1 μg/mL doxorubicin beginning 96 hrs post infection with viral vectors. U87MG, A172, and LNZ308 cells were treated for 24 hrs with 1 μg/mL doxorubicin and 100 μM temozolomide beginning 72 hrs post transfection with siRNAs. (B) FACS-based quantification of chemosensitivity. 96 hours post shRNA infection, U87MG samples were split in half and treated for 12 hours with either DMSO (light blue) or 1 μg/mL doxorubicin and 100 μM temozolomide (red). Live cells were collected and stained for 7AAD and Annexin-V. Data is represented as the percentage of Annexin V-positive 7AAD-negative cells in each sample, averaged over 2 experiments. P-values refer to student's two-tailed t-test used to compare doxorubicin and temozolomide-treated control to RIOK-shRNA cells. Validation of knockdown shown. FACS plots and raw data shown in Figure S15. (C) GBM301 cells treated with 25 μM ZVAD for 48 hrs beginning 3 days post-infection with viral vectors. Reduced phosphorylation of Akt on the TORC2 target site, Serine-473, is visible relative to total Akt protein. Reduced phosphorylation of several Akt targets, such as the FOXO3 transcription factor, is clear when phospho-epitope signal is compared to total protein controls. PARP cleavage is a read-out for apoptosis; PARP cleavage fragment in RIOK2 knockdown cells indicates residual caspase activity, due to the strong effect of RIOK2 loss. p53 upregulation was evident in GBM301 cells in the absence of residual caspase activity.

doi:10.1371/journal.pgen.1003253.g006

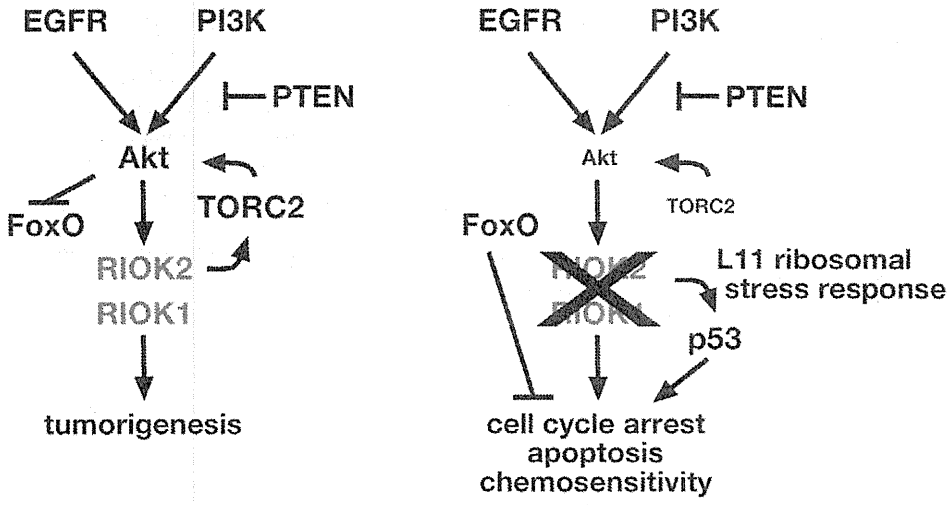

Figure 7. RIOK1 and RIOK2 are required for EGFR- and PI3K-mediated tumorigenesis. Pathway diagram placing RIOK1 and RIOK2 in relation to Akt downstream of EGFR and PI3K signaling in GBM. RIOK2 mediates signaling both upstream and downstream of Akt via stimulation of TORC2 (left). Loss of RIOK1 or RIOK2 reduces Akt signaling downstream of oncogenic EGFR and PI3K signaling, and induces the p53-dependent ribosomal stress checkpoint via RpL11 (right).
doi:10.1371/journal.pgen.1003253.g007

RpL11-p53-dependent ribosomal-stress checkpoint is associated with diseases caused by ribosomal protein haploinsufficiency, such as Diamond-Blackfan anemia, which are characterized by stem and progenitor cell failure [52,53]. Similarly, in *Drosophila*, haploinsufficiency of genes that encode ribosomal proteins retards developmental cell proliferation [62]. Given that cancer cells share many properties with stem and progenitor cells, induction of the RpL11-p53 ribosomal stress checkpoint may prove useful to deplete cancer cells. Indeed, recent experimental evidence indicates that the RpL11-p53-dependent ribosomal stress checkpoint suppresses tumorigenesis in mouse cancer models [63]. Moreover, several chemotherapeutic drugs induce the ribosomal stress checkpoint [64,65]. However, many of these drugs have deleterious effects unrelated to ribosomal stress, limiting their use. More specific induction of the ribosomal stress checkpoint, perhaps through RIO kinase inhibition, may prove therapeutically useful for GBM as well as related cancers.

The importance of RIO kinases in cancer cell survival has been validated in independent studies. RIOK2 was recently identified in an RNAi-based screen for kinases that are required for survival of glioma stem-like cells, which confirms our results, although the functionality of RIOK2 in glioma was not explored [66]. In addition, RIOK1 was identified in a cell-based RNAi screen for genes required for Ras-mediated cell survival, although the functionality of RIOK1 was not explored in this study [23]. Of note, almost all other published cell culture-based RNAi screens in GBM cell lines did not pick up RIOK1 or RIOK2 because these screens were not designed to distinguish between kinases that were required for genotypic-specific survival or growth of GBM cell lines, and instead focused on kinases that showed a common requirement in all glioblastoma cell lines tested, be they mutant or wild-type for p53, EGFR, or PTEN [67,68,69]. Our results, which are derived from independent multidisciplinary assays, are the first to establish functional connections between the RIO kinases, oncogenesis, Akt signaling, and the RpL11-p53-dependent ribosomal stress checkpoint (Figure 7). We envision that RIOK loss-of-function phenotypes in GBM cells are due to the combined effects of Akt inhibition and p53 induction, which together stimulate apoptosis and cell cycle exit of EGFR- and PTEN- mutant GBM cells, which share a common dependence on Akt signaling (Figure 7). Further studies to address the mechanisms by which the RIO kinases modulate Akt and p53 activity may lead to important new insights into the interactions between both of these pathways in both normal and cancer cells.

Materials and Methods

Fly stocks, genetics, culture conditions, immunohistochemistry, and gefitinib treatment

Flies were cultured at 25°C unless otherwise noted. Genotypes were established by standard genetics. Larval brain phenotypes were assessed and imaged as previously described [9]. Stocks were obtained from VDRC, NIG, and Bloomington stock centers (Table S1). *wor-Gal4* lines were from C. Doe. To create *UAS-ΔEGFR* constructs, a full-length human ΔEGFR cDNA was cloned into pUAS-T, and fly stocks with stable insertions were created.

The screen was based on crosses (see Text S1 for genetic methodology) that generated progeny containing a single RNAi construct exclusively expressed in GFP-labeled glia along with dEGFRλ and $dp110^{CAAX}$. Transgenes were overexpressed using the glial-specific *repo-Gal4* transcriptional driver. Screening was performed using fluorescence microscopy to visualize GFP-labeled glia in living larvae, and phenotypes were confirmed with confocal microscopy. Each positive-scoring RNAi construct was tested at least twice. Positive scoring RNAi constructs were also tested in wild-type glia, neuroblasts, and neurons (Text S1, Table S4)

Mammalian tissue culture techniques and RNAi

Established primary neurosphere cultures (gifts of H. Kornblum) were maintained as previously described in DMEM/F12 medium supplemented with bFGF and EGF [35,41]. Neurosphere cultures of GBM39 and GBM6 were created from serial xenografts of human GBMs (gifts of C.D. James). Cultured normal human glia were derived from a fresh surgical specimen of normal human cortex (gift of J. Olson) procured under a protocol approved by the Emory University institutional review board. Cultured mouse $PTEN^{-/-}$; $Ink4a/arf^{-/-}$ astrocytes (gift of R. Bachoo) were maintained in DMEM with 10% serum. The

RIOK2 cDNA (Origene) was overexpressed in *PTEN−/−; Ink4a/arf−/−* astrocytes from the pBabe retroviral vector.

The following drugs were used: Nutlin-3 (Cayman), MG132, Akt inhibitor IV (Calbiochem), temozolomide (Tocris), doxorubicin, rapamycin, PP242 (Santa Cruz), PI-103, ZVAD (Enzo), A443654 (gift of Greg Riggins), gefitinib (LC Laboratories), BEZ-235 (Biovision), LY294002 (Cell Signaling Technology), MK-2206, and GDC-0941 (Selleck). Doses of LY294002, BEZ-235, PI-103, GDC-0941, and MK-2206 used on GBM cells were determined by using dose response assays to find the concentrations at which cells showed substantial reduction (approximately <20% of normal) in Akt-mediated phosphorylation of PRAS40 (as detected by immunoblot).

Lentiviral shRNA pLKO.1 plasmids were obtained from the Broad Institute of MIT. RIOK1 shRNAs: TRCN0000196278 and TRCN0000196981. RIOK2 shRNAs: TRCN0000197250, TRCN0000196672, and TRCN0000196684. pLKO.1-GFP and a nontargeting shRNA against lacZ (in pLKO.1) were used as controls. Lentivirus was produced and used as per standard protocols (Sigma). Knockdown was evident by western blot 96 hrs post-infection. For neurosphere cultures, lentivirus was prepared in DMEM/F12 without serum, and infections were done on cells were plated adherently [36].

For siRNAs, all constructs were transfected at 50–100 μM with RNAimax (Invitrogen). Unless otherwise noted, siRNA-treated cells were harvested at 72 hrs post-transfection. 2 sets of pooled siRNAs were tested each for RIOK1 and RIOK2 (Dharmacon), and two different nontargeting siRNAs against GFP or luciferase were used as controls (Dharmacon). For knockdown of p53, p53 siRNAs were used and compared to matched control nontargeting siRNAs (Cell Signaling Technologies). Target sequences are listed in Text S1. For dual-knockdown experiments, U87MG cells were preferred because, with the necessary higher doses of siRNAs, U87MG-ΔEGFR cells showed nonspecific alterations in ΔEGFR expression that affected RIOK levels.

Immunoblot analysis

Cells were lysed in RIPA buffer and cleared lysates were subjected to standard immunobloting. The following primary antibodies were used: RIOK1 (Novus), RIOK2 (Sigma), p53 (Santa Cruz), p21, EGFR (BD), actin (DSHB), RpL11 (Invitrogen), NRBP2 (Abcam), STK17a/DRAK1 (Anaspec), PDGFRα, VRK1, CDK9, CDK7, STK17B/DRAK2, TLK1, phospho-Akt(S473), phospho-Akt(T308), phospho-PRAS40(T246), phospho-FOXO1(T24)/FOXO3(T32), Akt, phospho-NDRG1(T346), NDRG1, PRAS40, phospho-4E-BP1, 4E-BP1, PARP, cleaved caspase, FOXO3, TSC2, phospho-TSC2, mTor, phospho-mTor (T2448) (Cell Signaling Technologies)

WST1 and FACS assays

For WST-1 assays, cell lines were infected with lentiviral shRNA constructs and placed under selection for 48 hrs. Following selection, cells were plated for WST1 assays for cell proliferation/viability as per manufacturer's instructions (Clontech). For flow cytometry (FACS) analysis of DNA content, cells were dissociated and stained with propidium iodide (PI). For FACS analysis for apoptosis, cells were treated with indicated siRNAs or lentiviral vectors and stained with Annexin V-FITC and PI or 7AAD (Invitrogen, BD Biosciences). Assays were performed on a FACScaliber II flow cytometer and data were collected using FACSdiva software (BD Biosciences). Cell cycle profiles were generated using ModFit LT (Verity Software House). In all cases, at least 5000 cells were analyzed per sample.

RIOK2 overexpression and immunoprecipitation

293T cells were transiently transfected with Myc-DDK-tagged RIOK2 constructs. Cells were lysed in 50 mM HEPES pH 7.5, 150 mM NaCl, 5 mM EDTA, 1 mM DTT buffer with protease and phosphatase inhibitors [22]. RIOK2 was immunoprecipitated with M2-agarose (Sigma) from cleared lysates, and washed immunoprecipitates were subjected to immunobloting.

Biopsy lysates and immunohistochemistry on tumor samples

Human brain tumor biopsies and tissues were obtained from the Brain Tumor Translational Resource under a protocol approved by the University of California, Los Angeles institutional review board. Paraffin embedded human brain tumor specimens and tumor tissue microarrays with matched control tissue were prepared and sectioned using the UCLA Pathology Histology and Tissue Core Facility. Immunohistochemical staining was performed as previously described [70] or as specified by manufacturer guidelines (Sigma). The results were scored by neuropathologists according to standard clinical criteria, and images of RIOK2 immunoreactivity were taken on an Olympus DP72.

Mouse intracranial graft assays

For orthotopic implantation of mouse astrocytes engineered in vitro, low passage cells (no more than 8–10 passages) were used in two separate experiments. 1×10^5 cells in 5 μl of PBS were injected stereotactically 2 mm lateral to the midline and 1 mm anterior to the bregma into the brains of 5–6 week old athymic *nu/nu* mice. Mice were monitored and all animals were sacrificed upon evidence of neurological symptoms in experimental groups such that all samples were time-matched. Brains were removed for processing and histological analysis. Sections were scored independently by two neuropathologists for the presence of tumors and injection-associated needle scars. Animals injected with RIOK2-expresing cells that developed tumors outside of the brain (n = 1) were excluded from the final tally. All animal experiments were approved and conducted according to animal welfare guidelines of the IACUC at the University of California, San Diego.

Supporting Information

Figure S1 ΔEGFR signaling drives glial neoplasia. (A) Optical projections of whole brain-ventral nerve cord complexes from late 3rd instar larvae, approximately 130 hrs old, displayed at the same scale. Genotypes matched to those displayed in close-ups in B–G. Dorsal view; anterior up. Glia are labeled with GFP (green) driven by *repo-Gal4*. (B–G) 3 μm optical projections of brain hemispheres from late 3rd instar larvae, displayed at the same scale. Frontal sections, midway through brains. Anterior up; midline to left. Glial cell nuclei labeled with Repo (red); glial cell bodies labeled with GFP (green). Brains counter-stained with anti-HRP (blue), which reveals neuropil at high intensity and neuronal cell bodies at low intensity. (B, C) glial-specific overexpression of ΔEGFR in the larval brain induced excess glial cell numbers, brain enlargement, and lethality that was rescued with gefitinib (A, F, H). Co-overexpression of ΔEGFR with $dp110^{CAAX}$ produced lethal neoplasia, very similar to that of *dEGFRλ;dp110*^{CAAX} animals, that was partially suppressed by gefitinib treatment (A, D, G). However, gefitinib treatment did not fully suppress the growth of neoplastic ΔEGFR; $dp110^{CAAX}$ glia nor did it rescue lethality caused by ΔEGFR; $dp110^{CAAX}$ overexpression (G, H).
(TIF)

Figure S2 Classification of EGFR; PI3K modifiers. (A) Ven diagram comparing confirmed modifiers from this screen to other relevant RNAi-screens in *Drosophila* and to orthologous human kinases implicated in GBM, individual kinases noted in Table S6. (B, C) Network diagrams adapted from STRINGS showing functional connections between *Drosophila* modifier kinases (B), and functional connections between modifier kinases according to orthology information using COG (Clusters of Orthologous Groups) analysis (C) [26]. Confidence views of networks are presented such that stronger associations are represented by thicker lines. Orthologs of kinases implicated in GBM are shown in black, novel modifiers are shown in green (suppressors) and in red (enhancers). Many of the novel modifiers do not have established functional links to RTK or PI3K signaling in *Drosophila* (B). When network analysis takes into account datasets from orthologous kinases in other organisms, such as yeast (C), several of the novel modifiers show connections with each other and with other categorized modifiers of RTK and PI3K signaling, suggesting that these novel modifiers represent new pathway components.
(TIF)

Figure S3 Expression of human orthologs of modifier kinases in high-grade human gliomas. (A–F) Representative immunohistochemical stains for each indicated protein performed on high-grade malignant glioma tumor tissue, all done as part of the Human Protein Atlas Project. CDK7 and CDK9 are nuclear proteins, and show enriched immunoreactivity in tumor cells. TNK2 and RIOK2 are known or predicted cytoplasmic proteins. Antibodies were extensively validated as described in HPA [73], and this data is available at www.proteinatlas.org. Immunostains for each protein were performed on panels of 10–24 tumors, and this data is summarized in Table S10.
(TIF)

Figure S4 Expression of modifier orthologs in cultured GBM cells expressing ΔEGFR. U87MG and U87MG-ΔEGFR cells were cultured with .1% serum for 36 hrs to isolate ΔEGFR signaling, and their extracts were immunobloted for indicated proteins. ΔEGFR runs below full-length EGFR. Proteins that show upregulation in U87MG-ΔEGFR cells are each indicated with arrows.
(TIF)

Figure S5 RIO kinase expression in a panel of GBM cell lines. Indicated cell lines were cultured with .1% serum for 36 hrs to reduce expression artifacts from serum treatment, and their extracts were immunobloted for indicated proteins. PTEN mutant status is shown; SF767 is documented to be PTEN wild-type, while all others have been documented to be PTEN protein null mutant.
(TIF)

Figure S6 p110 and Akt inhibition, but not mTor inhibition, alters RIOK2 expression. (A) U87MG (parent) compared to U87MG-ΔEGFR cells, cultured in .1% serum and treated for 48 hrs with DMSO, 500 nM BEZ-235, or 2 μM PI-103, or treated for 24 hrs with DMSO or 1 μM A443654. PI3K inhibition by BEZ-235 and PI-103 shown by reduced Akt phosphorylation at Serine-473; the blot for Akt-Ser473 phosphorylation has been overexposed to highlight the degree of inhibition of PI3K signaling by BEZ-235 and other compounds rather than the differences in Akt-Ser473 phosphorylation between U87MG and U87MG-ΔEGFR (see Figure 2A). (B) U87MG compared to U87MG-ΔEGFR cells, cultured in .1% serum and treated for 24 hrs with DMSO (both U87MG and U87MG-ΔEGFR), 1 nM rapamycin, or 2 μM PP242, which is an inhibitor of mTor kinase activity. Inhibition of mTor kinase activity is evident by reduced Akt phosphorylation at Serine-473 and/or reduced 4E-BP1 phosphorylation. Increased 4E-BP1 phosphorylation was induced by rapamycin treatment, likely due to positive feedback [74]. RIOK2 is clearly elevated in the presence of EGFR, and is not decreased upon mTor inhibition. RIOK1 shows some reduction with PP242 treatment, but less so with rapamycin treatment.
(TIF)

Figure S7 Akt signaling regulates RIO kinase protein stability. (A) U87MG-ΔEGFR cells were infected with retroviruses containing PTEN, PTEN-G129R (catalytically inactive), or empty vector. Cells were serum-starved for 48 hours and treated for 8 hours with 10 μM MG132, a proteosomal inhibitor. Reduced Akt phosphorylation at Serine-473 is evidence of inhibition by PTEN. (B, C) U87MG-ΔEGFR (B) cells or GBM301 (C) cells were treated with DMSO or 2 μM A443654 with and without 10 μM MG132 for 10 hrs. Akt inhibition is evidenced by reduced PRAS40 phosphorylation in A443664 treated samples.
(TIF)

Figure S8 RIOK2 motif scan. The RIOK2 protein sequence was examined with the Scansite Motif Scanner (http://scansite.mit.edu/motifscan_seq.phtml) [75]. The kinase domain, which is highly similar to that of RIOK1 (RIO1), is indicated in blue. Potential phosphorylation sites are indicated by residue, and lower scores indicate that the predicted site falls into the top percentiles set by high stringency. Serine-483 in RIOK2 has been confirmed as a site of phosphorylation by several unpublished proteomic analyses available at PhosphoSitePlus (http://www.phosphosite.org) [76].
(TIF)

Figure S9 Potential phosphorylation of RIOK2 by Akt. Epitope-tagged RIOK2 (RIOK2-flag) was immunoprecipitated and detected by antibodies specific to Akt substrates phosphorylated on serine or threonine at characteristic Akt target sites (RXXS/T). RIOK2-KD-S483A-flag is an epitope tagged mutant form of RIOK2 which contains a serine-to-alanine change in Serine-483, which is a candidate Akt phosphorylation site (see Figure S8) and two point mutations that render RIOK2 kinase dead to block potential autophosphorylation [18]. Mutation of Serine-483 and the kinase domain did not block the ability of the Akt substrate antibody to detect RIOK2, indicating that other phosphorylation sites in RIOK2 are also recognized by the antibody.
(TIF)

Figure S10 RIOK2 expression in the giant cell and pseudopallisade fractions of GBM tumors. Immunohistochemical staining for RIOK2 (reddish brown), with hematoxilin counterstain. Wider views of heterogeneous RIOK2 immunoreactivity in ΔEGFR-positive human GBMs with giant cell components (A, B), cropped section of A also shown in Figure 4B. Wider view showing RIOK2 immunoreactivity in pseudopallisades (C), also shown cropped in Figure 4D, with high magnification (D) to show enrichment for RIOK2 present in the cellular fraction of pseudopallisades.
(TIF)

Figure S11 Akt and EGFR in GBM tumor tissues positive for RIOK2 expression. Immunohistochemical stains for EGFR and Akt done on sections from the same tumor samples stained for RIOK2 in Figure 4B/Figure S10A (A) and Figure 4E (B). Both tumors show strong expression of EGFR and phosphorylated Akt (Akt-S473-P).
(TIF)

Figure S12 WST1 proliferation assays reveal a requirement for modifier kinases in GBM cells. (A–C) WST-1 assays performed on U87MG cells for indicated genes. Following selection for shRNA expression, proliferation was measured with WST-1 reagent and quantified as the fold increase in absorbance between day 0 and day 3, normalized to controls treated with a nontargeting shRNA. 2–3 shRNAs tested per kinase. P values refer to one-way ANOVA with Dunnett post test.
(TIF)

Figure S13 RIOK knockdown verification for Figure 5. (A, B) Verification of RIOK1 and RIOK2 knockdown in U87MG (A) and U87MG-ΔEGFR (B) cells treated with the indicated shRNAs and subjected to WST1 assays as shown in Figure 5A (left panels). (C) Verification of RIOK2 knockdown in LNZ308 (C) cells treated with the indicated shRNAs and subjected to WST1 assays as shown in Figure 5A (right panel). (D, E) Verification of RIOK1 and RIOK2 knockdown in U87MG (D) and LNZ308 (E) cells treated with the indicated siRNAs and subjected to FACS analysis for cell cycle progression as shown in Figure 5B. (F) Upregulation of p53 upon RIOK2 knockdown with shRNAs. (G) Verification of p53 knockdown in U87MG cells treated with siRNAs against p53 and the RIOKs and subject to FACS analysis of apoptosis as shown in Figure 5E.
(TIF)

Figure S14 Loss of RIOK1 and RIOK2 induces L11-dependent p53 upregulation. RIOK1 or RIOK2 knockdown upregulates p53 and p21 expression in A712 (A) and U178 (B) GBM cells, which is blocked by concurrent RpL11 knockdown. A172 cells are PTEN-mutant and EGFR-mutant, U178 cells are PTEN-mutant, and both are wild-type for p53 [38,39,50]. For RpL11 co-knockdown experiments, cells were treated with equivalent amounts of siRNAs mixed 1:1 for all control and experimental samples. Cells were harvested 72 hrs post-transfection with siRNAs.
(TIF)

Figure S15 RIOK loss chemosensitizes GBM cells. Representative scatter plots of FACS-based quantification of chemosensitivity. U87MG cells were treated with 1 μg/mL doxorubicin and 100 μM temozolomide for 12 hrs beginning 96 hrs post shRNA infection. Treated cells were collected and stained live for 7AAD and Annexin-V. 7AAD alone identifies dead cells (Q1). Annexin V identifies cells in early apoptosis when alone (Q4) and in late stage apoptosis when coincident with 7AAD (Q2). Viable cells (Q3) stained for neither. The percentage of Annexin-V-positive cells present upon doxorubicin and temozolomide treatment significantly increased in RIOK1-shRNA and RIOK2-shRNA treated cells compared to cells treated with a non-targeting control shRNA.
(TIF)

Figure S16 Nutlin-3 treatment does not phenocopy RIOK2 loss. (A) U87MG cells treated with 10 μM nutlin-3 (red) or DMSO (control, black) for 48 hrs prior to fixation and propidium iodide staining for DNA content for cell cycle analysis by FACS. (B) Immunoblot showing that nutlin-3 treatment significantly increased p53 and p21 levels in U87MG cells, as compared to both control cells and siRNA-RIOK2 treated cells. (C) GBM301 cells plated adherently and infected with a GFP control lentivirus (left panel) or an shRNA lentivirus targeting RIOK2 (right panel). Brightfield images taken 96 hrs post-infection. RIOK2 protein levels drop starting about 72 hrs post-infection, such that 96 hrs is equivalent to 24 hrs of knockdown. Adherent GBM301 cells treated with 10 μM nutlin-3 for 24 hrs (middle panel). Nutlin-3 largely decreased growth of GBM301 cells, whereas RIOK2 knockdown more prominently stimulated apoptosis, yielding many pyknotic and vacuolated cells.
(TIF)

Figure S17 Loss of RIOK1 and RIOK2 function reduces TORC2-Akt signaling. (A) GBM6, a ΔEGFR-positive and p53 mutant neurosphere line. RIOK1 or RIOK2 knockdown caused reduced phosphorylation of Akt on the TORC2 target site, Serine-473, which is clear relative to total Akt protein. Cells harvested 5 days post-infection with viral vectors that target RIOK1/2 or a control vector, treated with 25 μM ZVAD for 48 hrs prior to harvest. (B) RIOK1 knockdown caused reduced phosphorylation of Akt on Serine-473 in U87MG-ΔEGFR cells. Reduced phosphorylation of FOXO3 at the TORC2-dependent Akt target site was detected upon RIOK1 knockdown. Cells harvested 5 days post-infection with viral vectors that target RIOK1/2 or a control vector, treated with 25 μM ZVAD for 48 hrs prior to harvest. (C) RIOK2 knockdown caused reduced phosphorylation of Akt on Serine-473 in U87MG cells. RIOK2 knockdown was also associated with reduced phosphorylation of NDRG1, aTORC2 read-out, and increased p53 protein levels. Cells treated with nontargeting control siRNAs or RIOK2 siRNAs, harvested 96 hrs post-transfection.
(TIF)

Figure S18 Expression of RIOK2 in other tumor types. (A–F) Representative immunohistochemical stains for RIOK2 performed on malignant tumor tissue, all done as part of the Human Protein Atlas Project [73]. (A) breast cancer (duct carcinoma), (B) lung cancer (squamous cell carcinoma), (C) colorectal cancer (adenocarcinoma), (D) head and neck cancer (squamous cell carcinoma), (E) prostate cancer (adenocarcinoma), and (F) malignant melanoma. RIOK2 showed strong expression in 92–100% of colon and head and neck tumors examined, in 50–58% of lung, prostate, and melanoma tumors examined, and in 25% of breast tumors examined (complete analysis and images available at www.protcinatlas.org).
(TIF)

Table S1 All kinases in the *Drosophila* genome. Kinases that are confirmed hits in the dEGFRλ;dp110^{CAAX} screen are in bold, kinases not tested due to lack of available constructs are in grey italics.
(XLS)

Table S2 Screen results from all UAS-dsRNA stocks tested. VDRC stock ID numbers prefaced by "v," Blooming stock ID numbers prefaced by "b," NIG stock ID numbers prefaced by an "n," TRIP stock numbers prefaced with a "t." Bold highlights all stocks that yielded reproducible genetic interactions and clear phenotypic alterations. Genes that are considered confirmed hits have multiple *UAS-dsRNA* stocks listed in bold and are highlighted in yellow. Key to genetic interactions: N: no interaction/no difference, WS: weak suppressor, S: moderate suppressor, SS: strong suppressor, WE: weak enhancer, E: moderate enhancer, SE: strong enhancer. "?" denotes interactions that were milder than the "weak" designation but subtly different from controls.
(XLS)

Table S3 Dominant negative constructs, overexpression constructs, and mutant alleles tested. Blooming stock ID numbers prefaced by "b." Bold highlights all confirmed stocks that yielded reproducible genetic interactions and clear phenotypic alterations. Key to genetic interactions: N: no interaction/no difference, WS: weak suppressor, S: moderate suppressor, SS: strong suppressor, WE: weak enhancer, E: moderate enhancer, SE: strong enhancer.

"?" denotes interactions that were milder than the "weak" designation but subtly different from controls.
(XLS)

Table S4 Testing modifier kinase RNAi constructs in wild-type glia, neuroblasts, neurons, and eye epithelia. VDRC stock ID numbers prefaced by "v," Blooming stock ID numbers prefaced by "b," NIG stock ID numbers prefaced by "n." Not all stocks tested in all assays. Bold highlights all confirmed dEGFRλ; $dp110^{CAAX}$ modifier stocks that yielded reproducible genetic interactions. Key to dEGFRλ; $dp110^{CAAX}$ genetic interactions: N: no interaction, WS: weak suppressor, S: moderate suppressor, SS: strong suppressor, WE: weak enhancer, E: moderate enhancer, SE: strong enhancer. "?" denotes interactions that were marginal. Testing in wild-type neuroblasts and neurons (2× *wor-Gal4*, *elav-Gal4*) was done with *UAS-dcr* in the background to potentiate RNAi. Data from RNAi constructs tested in neuroblasts with *insc-Gal4* derived from http://neuroblasts.imba.oeaw.ac.at 1. "Lethal," "semi-lethal," and "viable" refer to whole-animals effects of modifier constructs in an otherwise wild-type background. In glial-specific assays, whole animal lethality indicates that the genes in question may be essential for some aspect of normal glial function or development, but not necessarily for glial proliferation as blocking glial proliferation is not lethal. For analysis of larval glia, fixed specimens were stained for glial cell nuclei/numbers and viewed at higher magnification.
(XLS)

Table S5 *ΔEGFR* and *ΔEGFR;*$dp110^{CAAX}$ modifiers, listed by stocks tested. VDRC stock ID numbers prefaced by "v." Bold highlights all confirmed stocks that yielded reproducible genetic interactions and clear phenotypic alterations. Genes that are considered 'confirmed hits' in the initial screen are listed in bold. Key to genetic interactions: N: no interaction/no difference, WS: weak suppressor, S: moderate suppressor, SS: strong suppressor, WE: weak enhancer, E: moderate enhancer, SE: strong enhancer.
(XLSX)

Table S6 Human orthologs and functional classification of confirmed dEGFRλ;$dp110^{CAAX}$ modifier kinases. Orthologs were curated from http://kinase.com/ and names for each were updated according to current Gene ID numbers and NCBI annotations. GO terms from GOEast, http://omicslab.genetics.ac.cn/GOEAST/.
(XLS)

Table S7 Overlap with related RNAi screens in *Drosophila* and human systems. Novel modifier genes not previously implicated in glioblastoma are highlighted in green (suppressors) and red (enhancers). **Drosophila* genes that did not emerge from the annotated RNAi screens, but that have well established roles in RTK and PI3K signaling and/or cell proliferation and survival *in vivo*.
(XLS)

Table S8 Human Orthologs for novel modifiers of dEGFRλ;$dp110^{CAAX}$. Orthologs were curated from http://kinase.com/ and names for each were updated to current NCBI annotations. Human kinases selected for study in human GBM model systems are in bold, as are their *Drosophila* counterparts.
(XLS)

Table S9 TCGA Microarray data for human orthologs of novel modifiers. Each value is AgilentG4502A_07 log2 tumor/normal ratio taken from TCGA profiling, found at http://tcga-portal.nci.nih.gov/tcga-portal/AnomalySearch.jsp. Significant overexpression of 3-fold or more (>1.5) is noted in pink. Significantly decreased expression is noted in blue. Average expression for each gene for all samples is noted at the base of the table. Average expression with standard deviation for each gene for EGFR-overexpressors is noted at the base of the table.
(XLSX)

Table S10 Summary of Human Protein Atlas data adapted from www.proteinatlas.org. Genes highlighted in italics show notable upregulation in the indicated cells and tissues, as assessed by IHC.
(XLSX)

Text S1 Supplemental Results and Materials and Methods. Additional detail on validation of novel kinases in mammalian systems, screening methodology, and shRNA and siRNA sequences.
(DOC)

Acknowledgments

We thank Greg Riggins, Geoff Wahl, Mark Wade, Harley Kornblum, C. David James, Robert Bachoo, Daniel Brat, Chunhai Hao, Jeffrey Olson, and members of the Thomas, Cavenee and Mischel laboratories for useful discussions and/or reagents.

Author Contributions

Conceived and designed the experiments: RDR TRF JBT WKC FBF. Performed the experiments: RDR TRF GGG JW AI HY. Analyzed the data: RDR TRF JBT FBF WKC GGG JW SRV. Contributed reagents/materials/analysis tools: GGG IB PSM. Wrote the paper: RDR TRF. Edited the manuscript: RDR JBT WKC FBF.

References

1. Furnari FB, Fenton T, Bachoo RM, Mukasa A, Stommel JM, et al. (2007) Malignant astrocytic glioma: genetics, biology, and paths to treatment. Genes Dev 21: 2683–2710.
2. Nishikawa R, Ji XD, Harmon RC, Lazar CS, Gill GN, et al. (1994) A mutant epidermal growth factor receptor common in human glioma confers enhanced tumorigenicity. Proc Natl Acad Sci U S A 91: 7727–7731.
3. Mukasa A, Wykosky J, Ligon KL, Chin L, Cavenee WK, et al. (2010) Mutant EGFR is required for maintenance of glioma growth in vivo, and its ablation leads to escape from receptor dependence. Proc Natl Acad Sci U S A 107: 2616–2621.
4. Holland EC, Celestino J, Dai C, Schaefer L, Sawaya RE, et al. (2000) Combined activation of Ras and Akt in neural progenitors induces glioblastoma formation in mice. Nat Genet 25: 55–57.
5. Marumoto T, Tashiro A, Friedmann-Morvinski D, Scadeng M, Soda Y, et al. (2009) Development of a novel mouse glioma model using lentiviral vectors. Nat Med 15: 110–116.
6. Bachoo RM, Maher EA, Ligon KL, Sharpless NE, Chan SS, et al. (2002) Epidermal growth factor receptor and Ink4a/Arf: convergent mechanisms governing terminal differentiation and transformation along the neural stem cell to astrocyte axis. Cancer Cell 1: 269–277.
7. Holland EC, Hively WP, DePinho RA, Varmus HE (1998) A constitutively active epidermal growth factor receptor cooperates with disruption of G1 cell-cycle arrest pathways to induce glioma-like lesions in mice. Genes Dev 12: 3675–3685.
8. Cloughesy TF, Yoshimoto K, Nghiemphu P, Brown K, Dang J, et al. (2008) Antitumor activity of rapamycin in a Phase I trial for patients with recurrent PTEN-deficient glioblastoma. PLoS Med 5: e8. doi:10.1371/journal.pmed.0050008
9. Read RD, Cavenee WK, Furnari FB, Thomas JB (2009) A Drosophila model for EGFR-Ras and PI3K-dependent human glioma. PLoS Genet 5: e1000374. doi: 10.1371/journal.pgen.1000374
10. Reiter LT, Bier E (2002) Using Drosophila melanogaster to uncover human disease gene function and potential drug target proteins. Expert Opin Ther Targets 6: 387–399.
11. St Johnston D (2002) The art and design of genetic screens: Drosophila melanogaster. Nat Rev Genet 3: 176–188.
12. Dietzl G, Chen D, Schnorrer F, Su KC, Barinova Y, et al. (2007) A genome-wide transgenic RNAi library for conditional gene inactivation in Drosophila. Nature 448: 151–156.
13. Bellen HJ, Tong C, Tsuda H (2011) 100 years of Drosophila research and its impact on vertebrate neuroscience: a history lesson for the future. Nat Rev Neurosci 11: 514–522.

14. Freeman MR, Doherty J (2006) Glial cell biology in Drosophila and vertebrates. Trends Neurosci 29: 82–90.
15. LaRonde-LeBlanc N, Wlodawer A (2005) A family portrait of the RIO kinases. J Biol Chem 280: 37297–37300.
16. Vanrobays E, Gelugne JP, Gleizes PE, Caizergues-Ferrer M (2003) Late cytoplasmic maturation of the small ribosomal subunit requires RIO proteins in Saccharomyces cerevisiae. Mol Cell Biol 23: 2083–2095.
17. Widmann B, Wandrey F, Badertscher L, Wyler E, Pfannstiel J, et al. (2011) The kinase activity of human Rio1 is required for final steps of cytoplasmic maturation of 40S subunits. Mol Biol Cell.
18. Zemp I, Wild T, O'Donohue MF, Wandrey F, Widmann B, et al. (2009) Distinct cytoplasmic maturation steps of 40S ribosomal subunit precursors require hRio2. J Cell Biol 185: 1167–1180.
19. Baumas K, Soudet J, Caizergues-Ferrer M, Faubladier M, Henry Y, et al. (2012) Human RioK3 is a novel component of cytoplasmic pre-40S pre-ribosomal particles. RNA Biol 9: 162–174.
20. Strunk BS, Novak MN, Young CL, Karbstein K (2012) A translation-like cycle is a quality control checkpoint for maturing 40S ribosome subunits. Cell 150: 111–121.
21. Olsen JV, Blagoev B, Gnad F, Macek B, Kumar C, et al. (2006) Global, in vivo, and site-specific phosphorylation dynamics in signaling networks. Cell 127: 635–648.
22. Breitkreutz A, Choi H, Sharom JR, Boucher L, Neduva V, et al. (2010) A global protein kinase and phosphatase interaction network in yeast. Science 328: 1043–1046.
23. Luo J, Emanuele MJ, Li D, Creighton CJ, Schlabach MR, et al. (2009) A genome-wide RNAi screen identifies multiple synthetic lethal interactions with the Ras oncogene. Cell 137: 835–848.
24. Manning G, Plowman GD, Hunter T, Sudarsanam S (2002) Evolution of protein kinase signaling from yeast to man. Trends Biochem Sci 27: 514–520.
25. Morrison DK, Murakami MS, Cleghon V (2000) Protein kinases and phosphatases in the Drosophila genome. J Cell Biol 150: F57–62.
26. Szklarczyk D, Franceschini A, Kuhn M, Simonovic M, Roth A, et al. (2011) The STRING database in 2011: functional interaction networks of proteins, globally integrated and scored. Nucleic Acids Res 39: D561–568.
27. Bjorklund M, Taipale M, Varjosalo M, Saharinen J, Lahdenpera J, et al. (2006) Identification of pathways regulating cell size and cell-cycle progression by RNAi. Nature 439: 1009–1013.
28. Bettencourt-Dias M, Giet R, Sinka R, Mazumdar A, Lock WG, et al. (2004) Genome-wide survey of protein kinases required for cell cycle progression. Nature 432: 980–987.
29. Friedman A, Perrimon N (2006) A functional RNAi screen for regulators of receptor tyrosine kinase and ERK signalling. Nature 444: 230–234.
30. Boutros M, Kiger AA, Armknecht S, Kerr K, Hild M, et al. (2004) Genome-wide RNAi analysis of growth and viability in Drosophila cells. Science 303: 832–835.
31. Neumuller RA, Richter C, Fischer A, Novatchkova M, Neumuller KG, et al. (2011) Genome-Wide Analysis of Self-Renewal in Drosophila Neural Stem Cells by Transgenic RNAi. Cell Stem Cell 8: 580–593.
32. Sousa-Nunes R, Yee LL, Gould AP (2011) Fat cells reactivate quiescent neuroblasts via TOR and glial insulin relays in Drosophila. Nature 471: 508–512.
33. Reddy BV, Irvine KD (2011) Regulation of Drosophila glial cell proliferation by Merlin-Hippo signaling. Development 138: 5201–5212.
34. Huang HS, Nagane M, Klingbeil CK, Lin H, Nishikawa R, et al. (1997) The enhanced tumorigenic activity of a mutant epidermal growth factor receptor common in human cancers is mediated by threshold levels of constitutive tyrosine phosphorylation and unattenuated signaling. J Biol Chem 272: 2927–2935.
35. Laks DR, Masterman-Smith M, Visnyei K, Angenieux B, Orozco NM, et al. (2009) Neurosphere formation is an independent predictor of clinical outcome in malignant glioma. Stem Cells 27: 980–987.
36. Pollard SM, Yoshikawa K, Clarke ID, Danovi D, Stricker S, et al. (2009) Glioma stem cell lines expanded in adherent culture have tumor-specific phenotypes and are suitable for chemical and genetic screens. Cell Stem Cell 4: 568–580.
37. Lee J, Kotliarova S, Kotliarov Y, Li A, Su Q, et al. (2006) Tumor stem cells derived from glioblastomas cultured in bFGF and EGF more closely mirror the phenotype and genotype of primary tumors than do serum-cultured cell lines. Cancer Cell 9: 391–403.
38. Ishii N, Maier D, Merlo A, Tada M, Sawamura Y, et al. (1999) Frequent co-alterations of TP53, p16/CDKN2A, p14ARF, PTEN tumor suppressor genes in human glioma cell lines. Brain Pathol 9: 469–479.
39. Ciesielski MJ, Fenstermaker RA (2000) Oncogenic epidermal growth factor receptor mutants with tandem duplication: gene structure and effects on receptor function. Oncogene 19: 810–820.
40. Gallia GL, Tyler BM, Hann CL, Siu IM, Giranda VL, et al. (2009) Inhibition of Akt inhibits growth of glioblastoma and glioblastoma stem-like cells. Mol Cancer Ther 8: 386–393.
41. Pandita A, Aldape KD, Zadeh G, Guha A, James CD (2004) Contrasting in vivo and in vitro fates of glioblastoma cell subpopulations with amplified EGFR. Gene Chromosome Canc 39: 29–36.
42. Inda MD, Bonavia R, Mukasa A, Narita Y, Sah DW, et al. (2010) Tumor heterogeneity is an active process maintained by a mutant EGFR-induced cytokine circuit in glioblastoma. Genes Dev 24: 1731–1745.
43. Szerlip NJ, Pedraza A, Chakravarty D, Azim M, McGuire J, et al. (2012) Intratumoral heterogeneity of receptor tyrosine kinases EGFR and PDGFRA amplification in glioblastoma defines subpopulations with distinct growth factor response. Proc Natl Acad Sci U S A 109: 3041–3046.
44. Chen AJ, Paik JH, Zhang H, Shukla SA, Mortensen R, et al. (2012) STAR RNA-binding protein Quaking suppresses cancer via stabilization of specific miRNA. Genes Dev 26: 1459–1472.
45. Ying H, Zheng H, Scott K, Wiedemeyer R, Yan H, et al. (2010) Mig-6 controls EGFR trafficking and suppresses gliomagenesis. Proc Natl Acad Sci U S A 107: 6912–6917.
46. Guertin DA, Stevens DM, Thoreen CC, Burds AA, Kalaany NY, et al. (2006) Ablation in mice of the mTORC components raptor, rictor, or mLST8 reveals that mTORC2 is required for signaling to Akt-FOXO and PKCalpha, but not S6K1. Dev Cell 11: 859–871.
47. Sunayama J, Sato A, Matsuda K, Tachibana K, Watanabe E, et al. (2011) FoxO3a functions as a key integrator of cellular signals that control glioblastoma stem-like cell differentiation and tumorigenicity. Stem Cells 29: 1327–1337.
48. Tanaka K, Babic I, Nathanson D, Akhavan D, Guo D, et al. (2011) Oncogenic EGFR signaling activates an mTORC2-NF-kappaB pathway that promotes chemotherapy resistance. Cancer Discov 1: 524–538.
49. Bashir T, Cloninger C, Artinian N, Anderson L, Bernath A, et al. (2012) Conditional astroglial rictor overexpression induces malignant glioma in mice. PLoS ONE 7: e47741. doi:10.1371/journal.pone.0047741
50. Furnari FB, Lin H, Huang HS, Cavenee WK (1997) Growth suppression of glioma cells by PTEN requires a functional phosphatase catalytic domain. Proc Natl Acad Sci U S A 94: 12479–12484.
51. Vanrobays E, Gleizes PE, Bousquet-Antonelli C, Noaillac-Depeyre J, Caizergues-Ferrer M, et al. (2001) Processing of 20S pre-rRNA to 18S ribosomal RNA in yeast requires Rrp10p, an essential non-ribosomal cytoplasmic protein. EMBO J 20: 4204–4213.
52. Fumagalli S, Thomas G (2011) The role of p53 in ribosomopathies. Semin Hematol 48: 97–105.
53. Narla A, Ebert BL (2010) Ribosomopathies: human disorders of ribosome dysfunction. Blood 115: 3196–3205.
54. Simmons ML, Lamborn KR, Takahashi M, Chen P, Israel MA, et al. (2001) Analysis of complex relationships between age, p53, epidermal growth factor receptor, and survival in glioblastoma patients. Cancer Res 61: 1122–1128.
55. McLendon R, Friedman A, Bigner D, Van Meir EG, Brat DJ, et al. (2008) Comprehensive genomic characterization defines human glioblastoma genes and core pathways. Nature 455: 1061–1068.
56. Ohgaki H, Dessen P, Jourde B, Horstmann S, Nishikawa T, et al. (2004) Genetic pathways to glioblastoma: a population-based study. Cancer Res 64: 6892–6899.
57. Lowe SW, Ruley HE, Jacks T, Housman DE (1993) p53-dependent apoptosis modulates the cytotoxicity of anticancer agents. Cell 74: 957–967.
58. Stupp R, Mason WP, van den Bent MJ, Weller M, Fisher B, et al. (2005) Radiotherapy plus concomitant and adjuvant temozolomide for glioblastoma. N Engl J Med 352: 987–996.
59. Villalonga-Planells R, Coll-Mulet L, Martinez-Soler F, Castano E, Acebes JJ, et al. (2011) Activation of p53 by nutlin-3a induces apoptosis and cellular senescence in human glioblastoma multiforme. PLoS ONE 6: e18588. doi:10.1371/journal.pone.0018588
60. Zinzalla V, Stracka D, Oppliger W, Hall MN (2011) Activation of mTORC2 by association with the ribosome. Cell 144: 757–768.
61. Liu T, Deng M, Li J, Tong X, Wei Q, et al. (2011) Phosphorylation of right open reading frame 2 (Rio2) protein kinase by polo-like kinase 1 regulates mitotic progression. J Biol Chem 286: 36352–36360.
62. Marygold SJ, Roote J, Reuter G, Lambertsson A, Ashburner M, et al. (2007) The ribosomal protein genes and Minute loci of Drosophila melanogaster. Genome Biol 8: R216.
63. Macias E, Jin A, Deisenroth C, Bhat K, Mao H, et al. (2010) An ARF-independent c-MYC-activated tumor suppression pathway mediated by ribosomal protein-Mdm2 Interaction. Cancer Cell 18: 231–243.
64. Burger K, Muhl B, Harasim T, Rohrmoser M, Malamoussi A, et al. (2010) Chemotherapeutic drugs inhibit ribosome biogenesis at various levels. J Biol Chem 285: 12416–12425.
65. Sun XX, Dai MS, Lu H (2007) 5-fluorouracil activation of p53 involves an MDM2-ribosomal protein interaction. J Biol Chem 282: 8052–8059.
66. Goidts V, Bageritz J, Puccio L, Nakata S, Zapatka M, et al. (2012) RNAi screening in glioma stem-like cells identifies PFKFB4 as a key molecule important for cancer cell survival. Oncogene 31: 3235–3243.
67. Wurdak H, Zhu S, Romero A, Lorger M, Watson J, et al. (2010) An RNAi screen identifies TRRAP as a regulator of brain tumor-initiating cell differentiation. Cell Stem Cell 6: 37–47.
68. Wiedemeyer WR, Dunn IF, Quayle SN, Zhang J, Chheda MG, et al. (2010) Pattern of retinoblastoma pathway inactivation dictates response to CDK4/6 inhibition in GBM. Proc Natl Acad Sci U S A 107: 11501–11506.
69. Kim YW, Liu TJ, Koul D, Tiao N, Feroze AH, et al. (2011) Identification of novel synergistic targets for rational drug combinations with PI3 kinase inhibitors using siRNA synthetic lethality screening against GBM. Neuro Oncol 13: 367–375.
70. Mellinghoff IK, Wang MY, Vivanco I, Haas-Kogan DA, Zhu S, et al. (2005) Molecular determinants of the response of glioblastomas to EGFR kinase inhibitors. N Engl J Med 353: 2012–2024.

71. Raynaud FI, Eccles SA, Patel S, Alix S, Box G, et al. (2009) Biological properties of potent inhibitors of class I phosphatidylinositide 3-kinases: from PI-103 through PI-540, PI-620 to the oral agent GDC-0941. Mol Cancer Ther 8: 1725–1738.
72. Hirai H, Sootome H, Nakatsuru Y, Miyama K, Taguchi S, et al. (2010) MK-2206, an allosteric Akt inhibitor, enhances antitumor efficacy by standard chemotherapeutic agents or molecular targeted drugs in vitro and in vivo. Mol Cancer Ther 9: 1956–1967.
73. Uhlen M, Oksvold P, Fagerberg L, Lundberg E, Jonasson K, et al. (2010) Towards a knowledge-based Human Protein Atlas. Nat Biotechnol 28: 1248–1250.
74. Choo AY, Yoon SO, Kim SG, Roux PP, Blenis J (2008) Rapamycin differentially inhibits S6Ks and 4E-BP1 to mediate cell-type-specific repression of mRNA translation. Proc Natl Acad Sci U S A 105: 17414–17419.
75. Obenauer JC, Cantley LC, Yaffe MB (2003) Scansite 2.0: Proteome-wide prediction of cell signaling interactions using short sequence motifs. Nucleic Acids Res 31: 3635–3641.
76. Hornbeck PV, Kornhauser JM, Tkachev S, Zhang B, Skrzypek E, et al. (2011) PhosphoSitePlus: a comprehensive resource for investigating the structure and function of experimentally determined post-translational modifications in man and mouse. Nucleic Acids Res 40: D261–270.

mTOR Complex 2 Controls Glycolytic Metabolism in Glioblastoma through FoxO Acetylation and Upregulation of c-Myc

Kenta Masui,[1] Kazuhiro Tanaka,[1] David Akhavan,[1] Ivan Babic,[1] Beatrice Gini,[1] Tomoo Matsutani,[1] Akio Iwanami,[1] Feng Liu,[1] Genaro R. Villa,[1,2] Yuchao Gu,[1,2] Carl Campos,[3] Shaojun Zhu,[2] Huijun Yang,[1] William H. Yong,[4,5] Timothy F. Cloughesy,[4,5,6] Ingo K. Mellinghoff,[3] Webster K. Cavenee,[1,7] Reuben J. Shaw,[7,8] and Paul S. Mischel[1,7,9,*]
[1]Ludwig Institute for Cancer Research, University of California, San Diego, La Jolla, CA 92093, USA
[2]Department of Molecular and Medical Pharmacology, David Geffen School of Medicine at UCLA, Los Angeles, CA 90095, USA
[3]Human Oncology and Pathogenesis Program, Department of Neurology, Memorial Sloan-Kettering Cancer Center, New York, NY 10021, USA
[4]Henry Singleton Brain Tumor Program
[5]Jonsson Comprehensive Cancer Center
[6]Department of Neurology
David Geffen School of Medicine at UCLA, Los Angeles, CA 90095, USA
[7]Moores Cancer Center, University of California, San Diego, La Jolla, CA 92093, USA
[8]Molecular and Cell Biology Laboratory, Salk Institute for Biological Studies, La Jolla, CA 92037, USA
[9]Department of Pathology, University of California, San Diego, La Jolla, CA 92093, USA
*Correspondence: pmischel@ucsd.edu
http://dx.doi.org/10.1016/j.cmet.2013.09.013

SUMMARY

Aerobic glycolysis (the Warburg effect) is a core hallmark of cancer, but the molecular mechanisms underlying it remain unclear. Here, we identify an unexpected central role for mTORC2 in cancer metabolic reprogramming where it controls glycolytic metabolism by ultimately regulating the cellular level of c-Myc. We show that mTORC2 promotes inactivating phosphorylation of class IIa histone deacetylases, which leads to the acetylation of FoxO1 and FoxO3, and this in turn releases c-Myc from a suppressive miR-34c-dependent network. These central features of activated mTORC2 signaling, acetylated FoxO, and c-Myc levels are highly intercorrelated in clinical samples and with shorter survival of GBM patients. These results identify a specific, Akt-independent role for mTORC2 in regulating glycolytic metabolism in cancer.

INTRODUCTION

Metabolic reprogramming is a core hallmark of cancer (Ward and Thompson, 2012). Cancer cells convert the majority of their glucose into lactate, providing a supply of glycolytic intermediates as carbon-containing precursors for macromolecular biosynthesis. This biochemical adaptation (the Warburg effect) occurs even in the presence of sufficient oxygen to support oxidative phosphorylation (Dang, 2012b; Koppenol et al., 2011; Vander Heiden et al., 2009; Warburg, 1956) and enables cancer cells to meet the coordinately elevated anabolic and energetic demands imposed by rapid tumor growth (Tong et al., 2009). Uncovering the molecular circuitry by which the Warburg effect is activated and maintained may provide new insights into cancer pathogenesis that might be exploited through identification of new drug targets or detection of drug resistance mechanisms.

c-Myc is a critical regulator of cancer cell metabolism, including the Warburg effect (Dang et al., 2009). Here, we report an unexpected Akt-independent role for mTOR complex 2 (mTORC2) in regulating c-Myc levels and inducing metabolic reprogramming in glioblastoma (GBM), the most common and lethal form of brain cancer. We show that mTORC2 is required for the growth of GBM cells in glucose, but not galactose, and demonstrate that this is mediated by regulating the intracellular level of c-Myc. mTORC2 is shown to control these levels by Akt-independent phosphorylation of class IIa histone deacetylases (HDACs), which leads to the acetylation of FoxO1 and FoxO3, causing release of c-Myc from a suppressive miR-34c-dependent network. The net consequence of this series of events is the conferral of resistance to phosphatidylinositol 3-kinase (PI3K) and Akt inhibitor in vivo and shorter survival in patients.

RESULTS

mTORC2 Is Required for GBM Growth in Glucose through Myc-Dependent, Akt-Independent Signaling

To determine the role of mTORC2 in regulating glycolytic metabolism, we performed genetic depletion of mTORC2 using Rictor shRNA in GBM cells expressing *EGFRvIII*, a commonly mutated oncogene in GBM (Cancer Genome Atlas Research Network, 2008). EGFRvIII potently activates mTORC2 (p-Akt S473 and p-NDRG1 T346; Tanaka et al., 2011) and promotes glycolytic gene expression, tumor cell proliferation, and aerobic glycolysis (Babic et al., 2013; Guo et al., 2009; Figures S1A–S1C available online). In a dose-dependent fashion, Rictor shRNA knockdown suppressed the ability of GBM cells to grow in glucose, the effect

of which became apparent by day two, with increasing magnitude of effect by day three. In contrast, control and Rictor knockdown GBM cells displayed a similar proliferation rate by day three grown in galactose, a medium that reduces glycolytic flux and forces cells to rely on mitochondrial oxidative phosphorylation (Finley et al., 2011; Marroquin et al., 2007; Figure 1A). Further, Rictor overexpression rendered GBM cells exquisitely vulnerable to glucose deprivation or treatment with the glycolytic inhibitor 2-Deoxy-D-glucose (2-DG) (Figure 1B). Rictor shRNA knockdown also suppressed glycolytic gene expression (Figures 1C and 1D); significantly inhibited glucose consumption, lactate production, glutamine uptake, and glutamate secretion (Figures 1E and S1E); and limited tumor cell proliferation in an in vivo GBM xenograft model (Figure 1D). These results demonstrate that mTORC2 promotes glycolysis, enhancing the ability of GBM cells to grow in glucose, but also making them more dependent on glycolysis for survival.

c-Myc siRNA knockdown phenocopied the effect of mTORC2 genetic depletion on glycolytic gene expression (Figure S1D), raising the possibility that mTORC2 controls GBM glycolytic metabolism through c-Myc. Rictor siRNA knockdown suppressed c-Myc expression, whereas Rictor overexpression potently enhanced mTORC2 signaling and resulted in elevated c-Myc protein levels (Figure 1H). Most importantly, c-Myc siRNA knockdown completely abrogated the inhibitory effect of mTORC2 genetic depletion on glycolysis (Figures 1F and S1F). HIF-1α is also implicated as a key regulator of the glycolytic phenotype in cancer (Kaelin and Ratcliffe, 2008; Tong et al., 2009) and has been reported to be regulated by mTOR signaling (Hudson et al., 2002). In contrast to c-Myc, genetic depletion of HIF-1α by siRNA knockdown did not alter the inhibitory effect of mTORC2 genetic depletion on glucose consumption, lactate production, glutamine uptake, and glutamate secretion (Figures 1G and S1G). Taken together, these results demonstrate that mTORC2 regulates glycolytic metabolism in GBM cells through c-Myc.

mTORC2 is thought to control glycolytic metabolism through Akt (Dang, 2012b; Hagiwara et al., 2012; Plas and Thompson, 2005). However, Rictor knockdown almost completely suppressed c-Myc expression, whereas the effect of Akt or Raptor (mTORC1) depletion on c-Myc levels was modest (Figure 1I). These results raised the possibility that mTORC2 regulates c-Myc and resultant glycolytic metabolism in GBM cells independent of Akt or mTORC1.

mTORC2 Regulates c-Myc Level and Glycolysis through FoxO Acetylation

To identify an Akt-independent mechanism by which mTORC2 could regulate glycolytic metabolism, we examined two posttranslational modifications of the FoxO family of transcription factors. Inactivating phosphorylation by Akt and subsequent nuclear exclusion of FoxOs is a very well-described mechanism by which PI3K-activated tumor cells increase glycolysis (Biggs et al., 1999; Dang, 2012b), potentially by relieving suppression of c-Myc (Dang, 2012a; Ferber et al., 2012; Peck et al., 2013). We reasoned that an alternative posttranslational modification might be responsible for the Akt-independent regulation of FoxOs by mTORC2.

Pharmacologic inhibition of PI3K or Akt potently decreased FoxO phosphorylation, as expected (Figure 2A). However, surprisingly, elevated levels of acetylated FoxO, as well as increased expression of c-Myc, were detected using validated anti-acetyl-FoxO1 antibodies in GBM cells treated with LY294002 (pan-PI3K inhibitor) or Akti-1/2 (Akt inhibitor), raising the possibility of compensatory feedback regulation to maintain c-Myc expression through FoxO acetylation (Figure 2A). By an immnoprecipitation (IP) analysis, we determined that genetic depletion of mTORC2 by Rictor shRNA knockdown decreased the level of acetylated FoxO1 and FoxO3 (Figure 2B). Rictor knockdown also increased the formation of FoxO-DNA complexes (Figure 2C), enhanced FoxO target gene expression (Figure S2A), and regulated c-Myc and glycolytic gene expression in a FoxO-dependent fashion (Figures S2D and S2E). Conversely, Rictor overexpression increased the level of FoxO acetylation (Figure S2B) and suppressed the formation of FoxO-DNA complexes (Figure 2C). Taken together, these results suggest that mTORC2 controls c-Myc expression and glycolytic metabolism in GBM by regulating FoxO acetylation.

To better understand the role of FoxO acetylation in regulating mTORC2-dependent glycolytic metabolism, we employed a panel of FoxO plasmids that are mutated in key phosphorylation and/or acetylation sites (Biggs et al., 1999; Brunet et al., 2004; Nakamura et al., 2000; van der Horst and Burgering, 2007; Zhao et al., 2010; Figure 2D). These strategic constructs enabled us to compare the relative role of each posttranslational modification in regulating glycolytic metabolism. As expected, a phosphorylation-resistant mutant (FoxO1-3A), as well as another phosphorylation-resistant mutant (FoxO3-TM; data not shown), localized to the nucleus, suppressed c-Myc expression, and induced tumor cell apoptosis (Figures 2D and 2E). An acetylation-resistant mutant (FoxO1-5KR) and an analogous FoxO3 mutant (FoxO3-4KR; data not shown), were also localized to the nucleus, similarly suppressing c-Myc expression and inducing GBM cell apoptosis (Figures 2D and 2E), thus suggesting that either posttranslational modification of FoxO could regulate c-Myc expression. Therefore, we introduced a double mutant bearing residues that induce phosphorylation resistance and additional residues that mimic constitutive acetylation. This FoxO1-3A-5KQ construct, which was excluded from the nucleus, partially restored c-Myc levels and suppressed apoptosis induced by the FoxO1-3A mutant (Figure S2C). These results suggest a dominant role for FoxO acetylation relative to phosphorylation in regulating c-Myc and survival in GBM cells and suggest a dual-pronged mechanism of FoxO regulation that is conferred through two different posttranslational modifications. To determine whether FoxO acetylation was a critical determinant of the glycolytic phenotype of GBM cells, we assessed the impact of the acetylation-resistant mutant on glycolysis. Introduction of the FoxO1-5KR acetylation-resistant mutant decreased glycolysis, inhibiting glucose and glutamine uptake, and suppressed the secretion of lactate and glutamate (Figure 2F). Importantly, this inhibitory effect of the FoxO1-KR mutant on glycolysis was completely abrogated by c-Myc siRNA (Figure 2F). Further, upregulation of c-Myc by mTORC2 was also completely blocked by the FoxO1-5KR mutant (Figure 2G). Taken together, these results demonstrate that mTORC2 regulates c-Myc expression and glycolysis in GBM cells through FoxO acetylation.

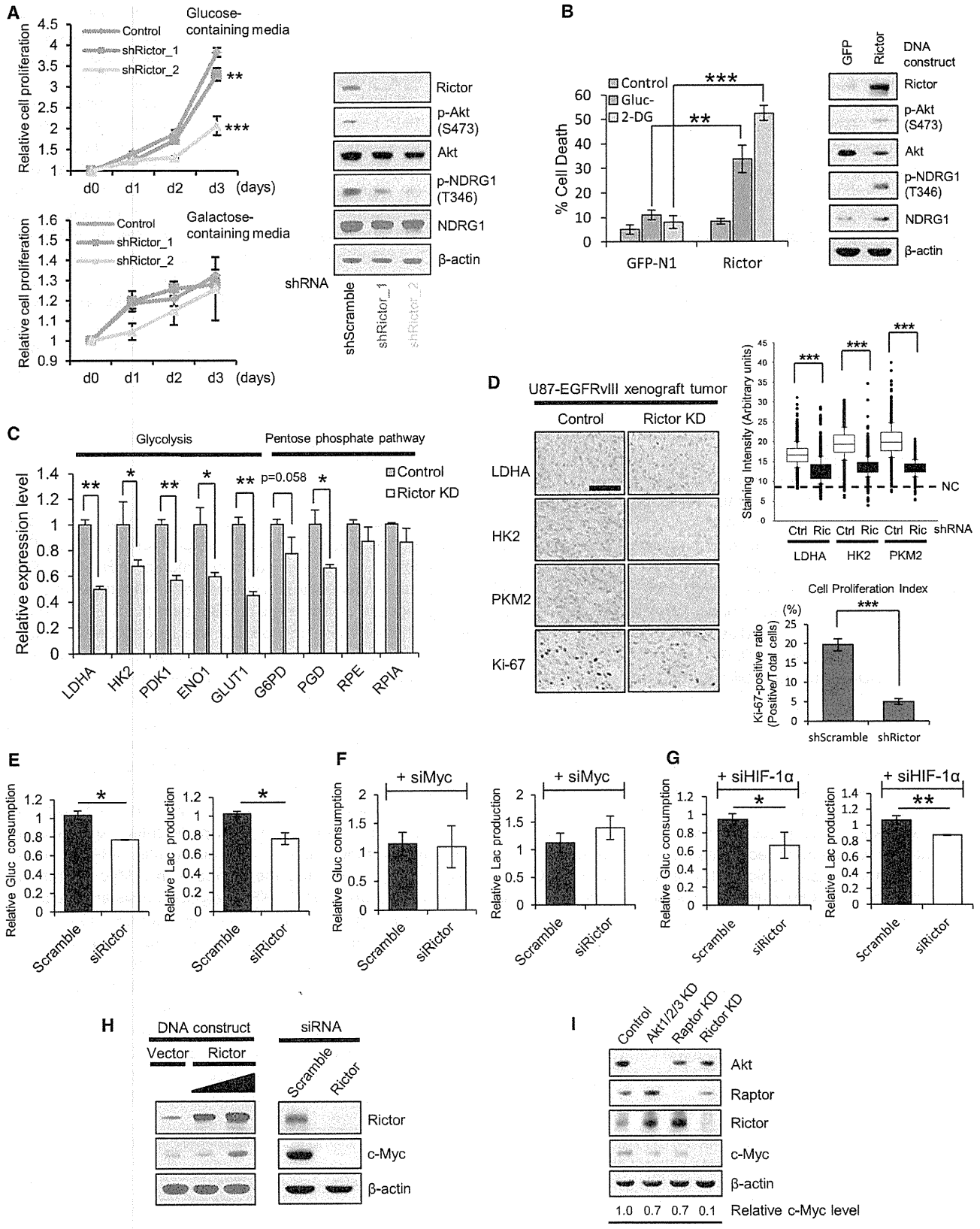

Figure 1. mTORC2 Is Required for GBM Growth in Glucose through c-Myc

(A) Growth curves of scramble or Rictor knockdown (KD) U87-EGFRvIII cells, cultured in media containing glucose or galactose. Error bars, ± SD. Immunoblot showing the verification of Rictor KD in U87-EGFRvIII cells.

(legend continued on next page)

mTORC2 Controls FoxO Acetylation through Class IIa HDACs, Independent of Akt

Acetylation of FoxOs is controlled, in part, through the balance between histone acetyltransferases (HATs) and HDACs (van der Horst and Burgering, 2007; Mihaylova et al., 2011; Wang et al., 2011). Gene expression microarray analysis identified only two genes from the HAT and HDAC families that were differentially expressed, *HDAC4* and *HDAC5* (class IIa HDACs), which were both significantly lower in EGFRvIII-expressing tumors with elevated mTORC2 signaling (Figure S3A). However, their level of downregulation in our cellular system was modest. Therefore, we focused on other, potentially more GBM-relevant mechanisms of regulation, including posttranslational modification (Mihaylova et al., 2011). We tested the possibility that mTORC2-dependent FoxO acetylation was mediated through inactivating phosphorylation of class IIa HDACs. Genetic depletion of mTORC2 with Rictor siRNA suppressed class IIa HDAC phosphorylation, concomitant with inhibition of FoxO acetylation and loss of c-Myc expression (Figure 3A). Conversely, Rictor overexpression markedly enhanced HDAC4, HDAC5, and HDAC7 phosphorylation (Figure 3B). Importantly, genetic depletion of Akt or Raptor (mTORC1) using siRNA knockdowns did not suppress class IIa HDAC phosphorylation or regulate levels of acetylated FoxO and c-Myc. Further, across a panel of GBM cell lines, the level of phosphorylation of HDAC4 was correlated with mTORC2 signaling (Figures 3C, S3B, and S3C). Additionally, the expression level of class IIa HDACs is inversely correlated with their phosphorylation status (Figures 3C and S3B), and future studies will be necessary to assess the possibilities that EGFR/mTORC2 signaling controls the level of class IIa HDACs by destabilizing them through phosphorylation (Potthoff et al., 2007) or decreasing their transcription (Figure S3A). These results demonstrate a specific role for mTORC2 in regulating class IIa HDAC phosphorylation in GBM that is independent of Akt. Notably, this mTORC2-HDAC-FoxO-Myc axis was also identified in other cancer types. In *EGFR*-mutant H1650 non-small-cell lung cancer cells, Rictor knockdown suppressed HDAC4 phosphorylation and abrogated expression of acetylated FoxO and c-Myc (Figure 3D). Further, pharmacological inhibition of Akt, mTORC1, and mTORC2 in H1650 cells, as well as in A549 non-small-cell lung cancer cells and HeLa cervical cancer cells, confirmed that suppression of mTORC2 signaling correlated with loss of FoxO acetylation and suppression of c-Myc and that these effects were clearly Akt independent (Figure S3D). These results do not exclude a role of mTORC1 in controlling c-Myc levels in other cancer types, but rather indicate that the mTORC2-dependent, Akt-independent, Myc-dependent pathway identified here may not be limited to GBM, but may be active in a broader range of cancer subtypes.

We next assessed the dependence of GBM cells on class IIa HDACs for regulation of FoxO acetylation and Myc expression. Knockdown of class IIa HDACs increased FoxO acetylation and c-Myc expression (Figure 3E), impairing FoxO transcriptional activity (Figure 3F). Genetic depletion of class IIa HDACs with siRNA knockdown, or pharmacological inhibition of class IIa HDACs, abrogated the effect of Rictor knockdown on c-Myc expression (Figures S3E and S3F), indicating that mTORC2 regulates c-Myc through class IIa HDACs. Further, the acetylation-resistant FoxO1-5KR mutant prevented c-Myc upregulation in response to knockdown of class IIa HDACs (Figure 3G), confirming that class IIa HDACs regulate c-Myc through FoxO acetylation. More importantly, knockdown of class IIa HDACs promoted GBM cell proliferation, which was reversed by c-Myc codepletion (Figure 3H). Taken together, the findings demonstrate that inactivating phosphorylation of class IIa HDACs by mTORC2 controls FoxO acetylation and c-Myc levels, promoting GBM proliferation.

Acetylated FoxO Regulates c-Myc through miR-34c

FoxOs antagonize c-Myc (Dang, 2012a; Ferber et al., 2012; Peck et al., 2013), possibly by increasing the expression of miR-145 (Gan et al., 2010) and miR-34c (Kress et al., 2011), limiting c-Myc mRNA stability and translation. In GBM cells, miR-145 and miR-34c levels were both suppressed by FoxO1/FoxO3 knockdown (Figure 4A), and introduction of miR-34c, miR-145, or their anti-miR constructs demonstrated that these two microRNAs regulate c-Myc levels in GBM cells (Figure 4B). To determine whether these microRNAs are independently regulated by differential posttranslational modifications of FoxO, we took advantage of the FoxO phosphorylation and acetylation mutants. Introduction of the FoxO phosphorylation-resistant mutant (FoxO1-3A) into GBM cells upregulated expression of miR-145, but not miR-34c (Figure 4C). In contrast, introduction of the acetylation-resistant mutant (FoxO1-5KR) increased the expression of miR-34c, but not miR-145 (Figure 4C). Chromatin immunoprecipitation (ChIP) analysis further showed that the FoxO1-5KR acetylation-resistant mutant was preferentially enriched in the miR-34c promoter regions, but not in the miR-145 promoter region (Figure 4D), and the decrease in c-Myc expression in response to the FoxO1-5KR acetylation-resistant mutant was reversed by anti-miR-34c, but not by anti-miR-145 (Figure 4E). Furthermore, mTORC2 activation resulted in a decrease in miR-34c expression, but not miR-145 expression (Figure 4F), while Rictor knockdown partially restored the suppression of c-Myc by anti-miR-34c, but not by anti-miR-145 (Figure 4G). The effect of anti-miR-34c on c-Myc expression in the setting of Rictor depletion is limited, suggesting that, in addition to the miRNA regulation, there may exist other functions of Rictor in control of c-Myc, considering the fact that the expression and

(B) Cell deaths of GFP- or Rictor-overexpressing U87 cells after 48 hr treatment with glucose deprivation (Gluc−) or the glycolytic inhibitor, 2-Deoxy-D-glucose (2-DG, 10 mM). Immunoblot showing the verification of Rictor overexpression in U87 cells.
(C) mRNA levels of glycolysis and pentose phosphate pathway (PPP) enzymes in control or Rictor KD U87-EGFRvIII cells.
(D) Cell-based immunohistochemical analysis for glycolytic enzymes and a proliferative marker Ki-67 in U87-EGFRvIII xenograft tumors with scramble or Rictor shRNA (n = 3). Scale bar, 50 μm. NC denotes the averaged staining intensity obtained by negative control of each sample.
(E–G) Relative glucose consumption and lactate production in control versus Rictor KD U87-EGFRvIII cells (E), combined with c-Myc KD (F) or HIF-1α KD (G).
(H) Biochemical analysis of c-Myc expression for Rictor overexpression in U87 cells and Rictor KD in U87-EGFRvIII cells.
(I) Immunoblot analysis of c-Myc in U87-EGFRvIII cells with indicated siRNAs regarding Akt, mTORC1 (Raptor), and mTORC2 (Rictor).
All error bars, except growth curves (A), SEM. See also Figure S1.

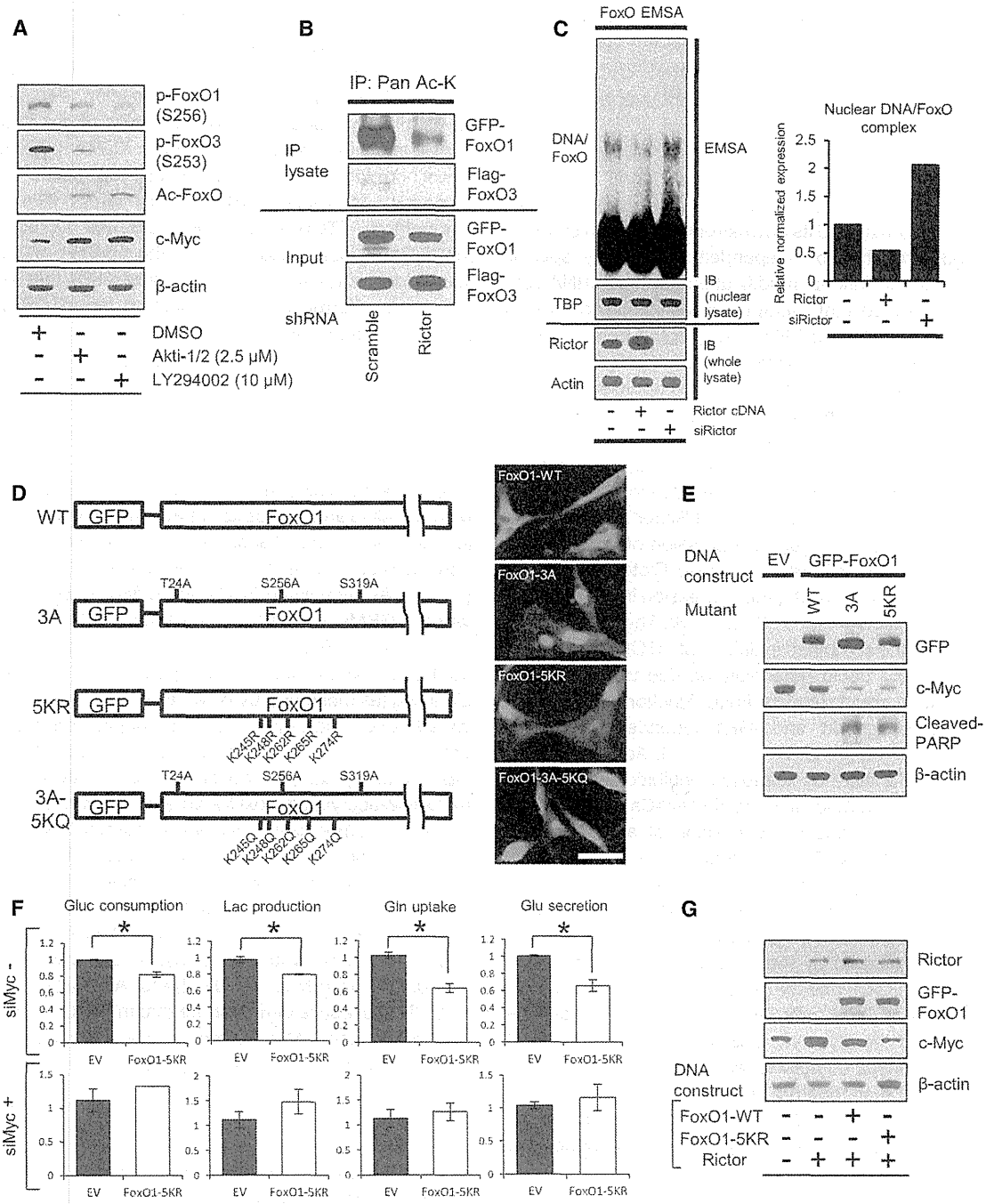

Figure 2. mTORC2 Regulates c-Myc and Glycolysis through FoxO Acetylation

(A) Phosphorylated FoxO, acetylated FoxO, and c-Myc protein levels in U87-EGFRvIII treated with Akt inhibitor (Akti-1/2) or Pan-PI3K inhibitor (LY294002) for 24 hr.

(B) IP analysis of the association of acetyl-lysine (Ac-K) with FoxO plasmids in U87-EGFRvIII cells, which were cotransfected with GFP-FoxO1 and Flag-FoxO3 and depleted with or without Rictor.

(C) EMSA assay, with the use of nuclear extracts from U87 with Rictor overexpression or Rictor KD, showing the DNA/FoxO-protein EMSA complex. Immunoblots for TATA binding protein (TBP) were used to normalize protein loading for nuclear extracts. Quantitative bar graph demonstrated relative DNA/FoxO complex levels in each group.

(D) Schematic illustration of GFP-FoxO1 mutants: 3A, Akt-mediated phosphorylation resistant; 5KR, acetylation resistant; and 5KQ, constitutively acetylated. Immunofluorescent images representing U87-EGFRvIII cells expressing GFP-FoxO1 and mutants. Scale bar, 20 μm.

(E) Immunoblot analysis on the effects of wild-type FoxO1, FoxO1-3A, and FoxO1-5KR on c-Myc and cleaved PARP.

(F) Relative glucose consumption, lactate production, glutamine uptake, and glutamate secretion in empty vector or FoxO1-5KR mutant overexpressing U87-EGFRvIII cells with or without depletion of c-Myc.

(G) Immunoblot assessment of c-Myc in U87 cells cotransfected with Rictor-expressing vector and wild-type/mutant FoxO-expressing vector.

Error bars, SEM. See also Figure S2.

activity of c-Myc are regulated by a variety of factors at the multiple levels (Albihn et al., 2010; Liu and Levens, 2006). Taken together, these results indicate that acetylated FoxO increases c-Myc levels by relieving miR-34c-dependent suppression.

Resistance to PI3K and Akt Inhibitors Is Mediated by mTORC2-Dependent Acetylation of FoxO and Consequent Maintenance of c-Myc Levels

Having shown that FoxO and its downstream regulation of c-Myc are controlled through two independent and highly specific pathways of posttranslational modification and microRNA suppression, we reasoned that therapeutic resistance to PI3K or Akt inhibitors by sustained c-Myc activity could be one critical and potentially clinically actionable consequence. To test this hypothesis, we examined the effect of pharmacologic inhibition of PI3K or Akt on FoxO acetylation, c-Myc expression, and tumor cell survival. Treatment of GBM cells with LY294002 or Akti-1/2 suppressed PI3K and Akt signaling, respectively, but failed to promote FoxO target gene expression, concomitant with a compensatory elevation in p-NDRG1 and Rictor levels (Figures 5A, 5B, and S4A). This continued suppression of FoxO activity was mediated through mTORC2, because Rictor knockdown markedly elevated FoxO target gene expression in the presence of PI3K or Akt inhibition (Figures 5B and S4A). The restoration of FoxO activities by the combined inhibition of mTORC2 and PI3K/Akt was striking and could potentially be due to the fact that mTORC2 inhibition could regulate FoxO function both through acetylation and through Akt- and SGK1-dependent phosphorylation (Guertin et al., 2006; Zhao et al., 2011). Additionally, this recovery of FoxO activity by combined inhibition of PI3K/Akt and mTORC2 was reversed by class IIa HDACs inhibition to a greater degree than it was by expression of a constitutively active form of Akt (HA-Akt-E17K), suggesting the dominance of acetylation in regulating FoxO transcriptional activity (Figures S4B and S4C). Importantly, treatment of GBM cells with PI3K or Akt inhibitors significantly elevated c-Myc levels, and this was completely reversed by the acetylation-resistant FoxO1-5KR mutant (Figure 5C), and by Rictor knockdown (Figure 5D). Further, treatment of GBM cells with Akti-1/2 actually increased the mRNA level of the glycolytic enzymes *LDHA*, *HK2*, *PDK1*, and *GLUT1*, which was completely abrogated by Rictor knockdown (Figure 5E). Taken together, these results strongly indicate that GBM cells treated with PI3K or Akt inhibitors maintain c-Myc levels and enhanced glycolysis through mTORC2 feedback-promoted FoxO acetylation.

Combined Inhibition of PI3K/Akt and mTORC2 Suppresses Acetylated FoxO-c-Myc Signaling and Promotes Tumor Cell Death

If mTORC2-dependent FoxO acetylation maintains c-Myc levels to drive PI3K or Akt inhibitor resistance, then combined suppression of mTORC2 and PI3K or Akt should decrease cellular levels of c-Myc, potentially causing tumor cell death. Consistent with this hypothesis, Rictor shRNA knockdown synergized with LY294002 or Akti-1/2 to cause GBM tumor cell death (Figures 6A and 6B). Therefore, we asked whether dual pharmacologic inhibition of PI3K and mTOR kinase could also suppress FoxO acetylation, decrease c-Myc levels, lower glycolytic enzyme expression, and cause tumor cell death. To test this, we treated the patient-derived GBM xenograft model TS516 (Rohle et al., 2013) with the dual PI3K/mTOR inhibitor XL765 (SAR245409) (Figure 6C). XL765 inhibited mTORC2 signaling, blocked FoxO acetylation, increased miR-34c expression, decreased cellular levels of c-Myc, and reduced expression of glycolytic enzymes LDHA and HK2. Most importantly, XL765 potently reduced tumor growth, inducing tumor cell apoptosis (Figure 6C). Currently, no specific mTORC2 inhibitors exist, and ATP-competitive mTOR kinase inhibitors like XL765 also affect mTORC1 signaling. However, in the context of the mTORC2 knockdown experiments (Figures 6A and 6B), these results indicate that pharmacological inhibition of mTORC2 prevents c-Myc-dependent PI3K inhibitor resistance (Dang, 2012a; Ilic et al., 2011; Muellner et al., 2011) through inhibition of FoxO acetylation.

mTORC2/Acetylated FoxO/c-Myc Alterations in Clinical Human GBMs

To explore the clinical implications of mTORC2-acetylated FoxO-Myc signaling and assess its impact on prognosis, we performed immunohistochemical analysis of a tissue microarray (TMA) that contained 26 normal brain samples and 80 GBM tumor samples (Figure 7A). Acetylated FoxO and c-Myc were both highly elevated in GBMs relative to normal brain (Ac-FoxO, $p = 0.013883$; c-Myc, $p = 9.58832E-05$), being individually upregulated in 45.0% and 58.8% of tumors, respectively (Figure 7A). mTORC2 signaling (as measured by p-NDRG1; Tanaka et al., 2011), acetylated FoxO, and c-Myc were also highly correlated with each other (Figures 7B–7D, S5A, and S5B). Immunoblot analysis of GBM autopsy samples confirmed coordinate increases in the mTORC2-acetylated FoxO-Myc axis, as well as glycolytic enzymes, in tumor tissue relative to normal brain (Figures S5C and S5D), and elevated acetylated FoxO and c-Myc were found to be highly correlated (Spearman's rank correlation coefficient, $r^2 = 0.8288$) in this limited number of autopsy samples ($n = 8$). Finally, elevated acetylated FoxO and c-Myc on TMA were significantly associated with shorter overall survival in GBM patients ($p = 0.0367$ for c-Myc, $p = 0.0799$ for Ac-FoxO; Figures 7E and S5E). These results demonstrate that mTORC2 signaling, acetylated FoxO, and c-Myc expression are coordinately upregulated in GBM patients with worse prognoses (Figure 7F).

DISCUSSION

The Warburg effect enables cancer cells to obtain a sufficient supply of macromolecular precursors required for rapid cellular proliferation while still meeting their energy requirements (Tong et al., 2009). c-Myc plays a central role in regulating this metabolic hallmark of cancer (Cairns et al., 2011; DeBerardinis et al., 2008; Koppenol et al., 2011; Levine and Puzio-Kuter, 2010; Vander Heiden et al., 2009; Ward and Thompson, 2012). Although many receptor signaling pathways, including Wnt, Shh, Notch, TGF-β, and RTK signaling through the PI3K pathway, have been implicated in Myc upregulation (Dang, 2012a), the mechanisms by which mutated growth factor receptor signaling pathways engage c-Myc remain incompletely understood.

We recently showed that EGFRvIII regulates glycolytic metabolism and tumor growth through hnRNPA1-dependent

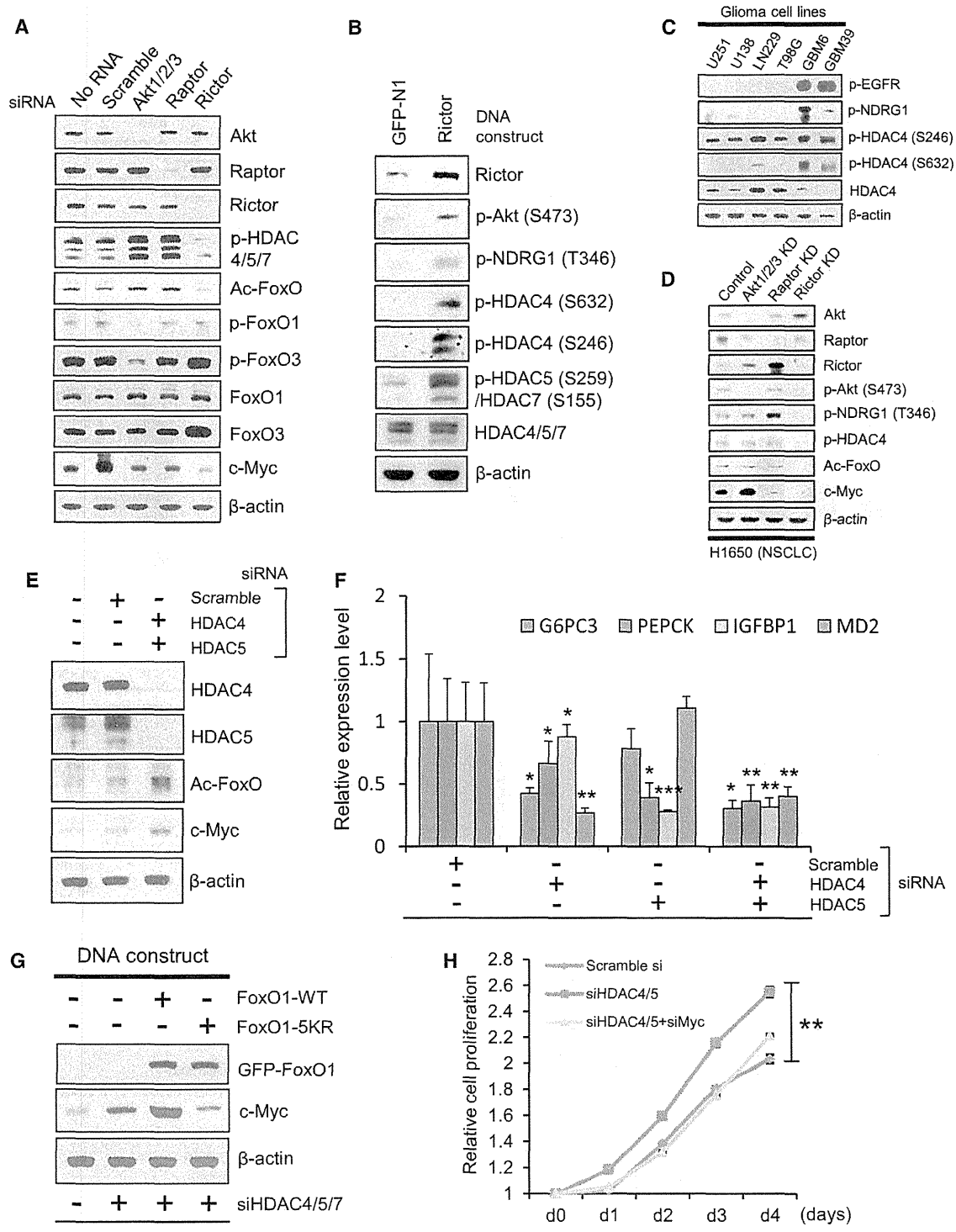

Figure 3. mTORC2 Controls FoxO Acetylation through Class IIa HDACs, Independent of Akt

(A) Immunoblot analysis of c-Myc, phosphorylated HDAC, and several forms of FoxO in U87-EGFRvIII cells with indicated siRNAs regarding Akt and mTOR complex.

(B) Immunoblot showing change in phosphorylated class IIa HDACs from U87 cells overexpressing GFP or Rictor DNA plasmids.

(C) Immunoblot analysis for the status of p-EGFR, p-NDRG1, and class IIa HDACs in several glioma cell lines.

(D) Immunoblot analysis of phosphorylated HDAC, acetylated FoxO, and c-Myc in *EGFR*-mutated, non-small-cell lung cancer (NSCLC) cells (H1650) with indicated KD regarding Akt and mTOR complex.

(E) Immunoblot showing change of acetylated FoxO and c-Myc in U87 cells with indicated siRNAs against class IIa HDACs.

(F) qRT-PCR from U87 cells of FoxO target genes following siRNA-mediated depletion of HDAC4/5.

(legend continued on next page)

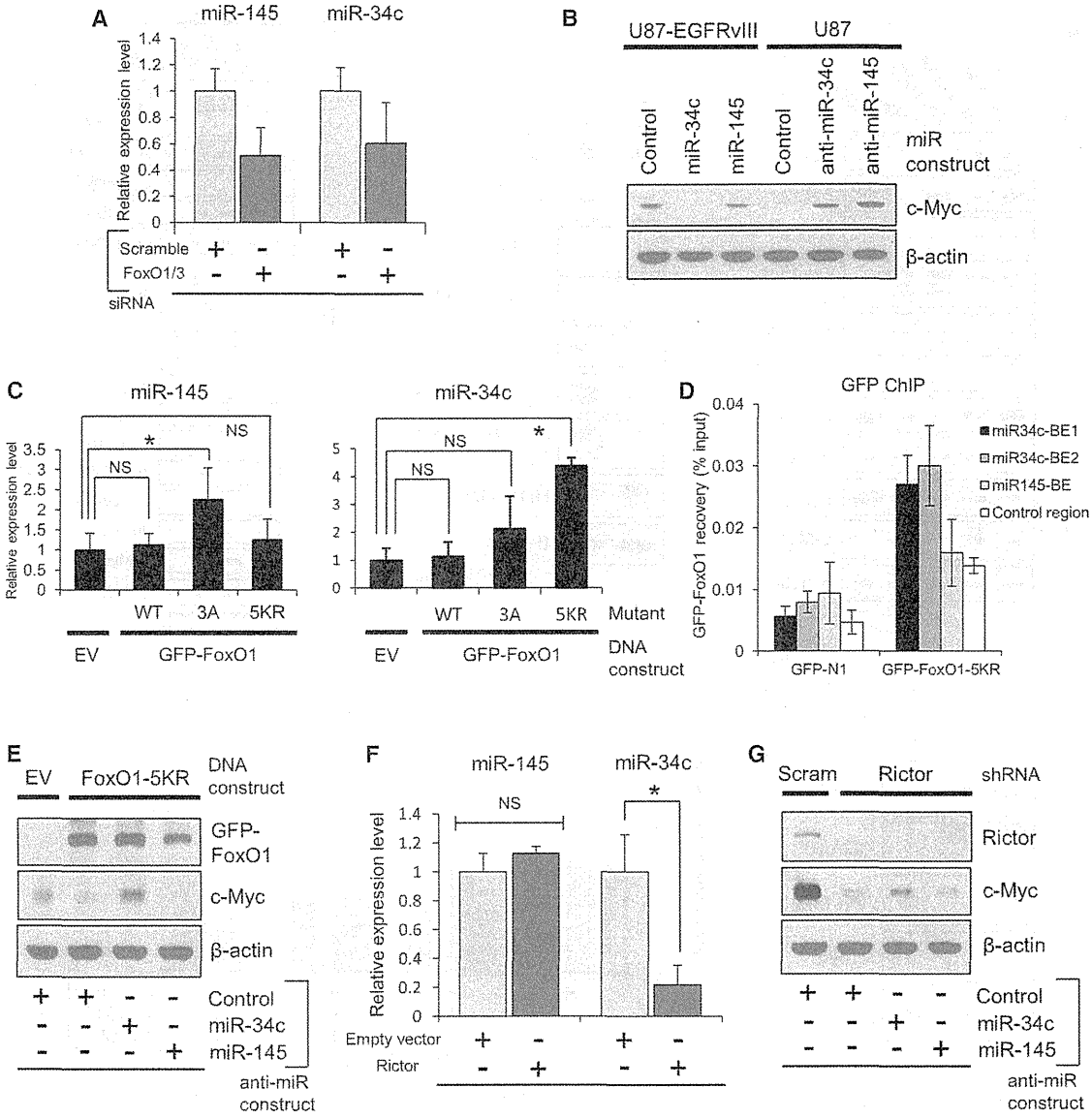

Figure 4. Acetylated FoxO Regulates c-Myc through miR-34c

(A) Relative expression of miR-145 and miR-34c in scramble versus FoxO KD U87 cells.

(B) Myc protein levels in U87-EGFRvIII cells with miRNA mimics and U87 with miRNA inhibitors.

(C) Relative expression changes of miR-145 and miR-34c in U87-EGFRvIII cells transfected with indicated FoxO plasmids.

(D) ChIP analysis on U87-EGFRvIII cells transfected with control vector or GFP-FoxO1-5KR and assessed for GFP-FoxO1 recovery on binding elements (BEs) in miR-34c promoter (Kress et al., 2011) and miR-145 promoter (Gan et al., 2010) regions.

(E) 5KR-FoxO1-mediated downregulation of c-Myc was reverted by the inhibition of miR-34c, but not miR-145, in U87-EGFRvIII cells.

(F) mRNA changes of miR-145 and miR-34c in U87 cells transfected with empty vector (EV) or Rictor-expressing vector.

(G) Immunoblot assessment of c-Myc change in U87-EGFRvIII cells cotransfected with shRictor and miRNA inhibitors.

Error bars, SEM.

alternative splicing of the Myc binding partner Max (Babic et al., 2013). This alternatively spliced product, Delta Max, promotes GBM cell proliferation in glucose and is required for tumor growth in a Myc-dependent fashion (Babic et al., 2013). Taken together with the results presented here, a model is emerging in which aberrant growth factor receptor signaling in GBM engages c-Myc signaling through two complementary and interlacing mechanisms: (1) alternative splicing of Delta Max

(G) Immunoblot showing c-Myc amount from U87 cells bearing siRNAs against class IIa HDACs, combined with overexpression of FoxO DNA plasmids.

(H) Cell proliferation assay of scramble or class IIa HDAC KD U87 cells, combined with or without c-Myc depletion. $p < 0.01$ for comparison between siHDAC cells and scramble siRNA cells, or siHDAC/siMyc cells. Error bars, ± SD.

All error bars, except growth curves (H), SEM. See also Figure S3.

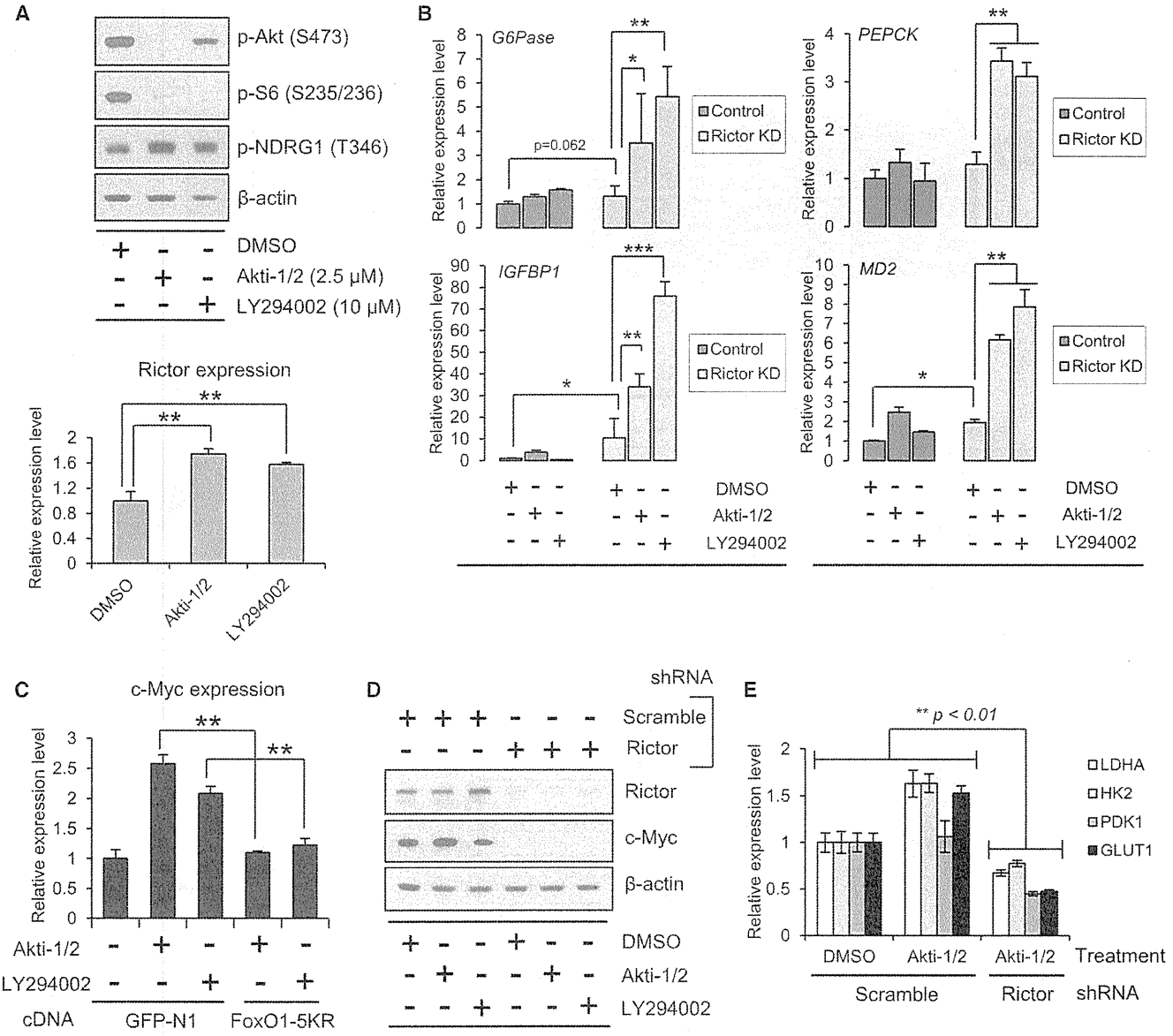

Figure 5. Resistance to PI3K and Akt Inhibitors Is Mediated by mTORC2-Dependent Acetylation of FoxO and Consequent Maintenance of c-Myc

(A) mTORC2 activation under Akt/PI3K inhibition in U87-EGFRvIII cells shown by western blotting for p-NDRG1 protein and qRT-PCR for Rictor mRNA.

(B) qRT-PCR analysis for FoxO target genes in U87-EGFRvIII cells treated by PI3K/Akt inhibitors for 24 hr, combined with or without Rictor KD. Targeting both PI3K/Akt and mTORC2 dramatically restores FoxO activity.

(C) qRT-PCR from U87-EGFRvIII cells of c-Myc gene following treatment with PI3K/Akt inhibitor, transfected with or without FoxO1-5KR.

(D) Immunoblot assessment of c-Myc in U87-EGFRvIII cells treated by PI3K/Akt inhibitors, combined with or without Rictor KD.

(E) mRNA levels of Myc-regulated metabolic enzymes in U87-EGFRvIII cells treated by an Akt inhibitor, combined with or without Rictor KD.

Error bars, SEM. See also Figure S4.

(Babic et al., 2013) to modulate c-Myc function and (2) control of cellular levels of c-Myc through mTORC2, as demonstrated here. Importantly, both mechanisms are required for GBM growth through their effects of Myc-dependent glycolytic metabolism, because genetic depletion of either Delta Max (Babic et al., 2013) or mTORC2 (Figure 1) blocks the ability of GBM cells to utilize glucose, but not galactose, for tumor cell proliferation in a c-Myc dependent fashion. These mechanisms also appear to be cooperative, acting at different points of c-Myc regulation, thus highlighting the role for c-Myc in GBM pathogenesis and suggesting that its pathogenicity, at least in part, may be mediated through upregulation of glycolytic metabolism.

A surprising implication of this study arises from the observation that GBM cells treated with PI3K or Akt inhibitors maintain c-Myc levels and enhanced glycolysis through mTORC2 feedback-promoted FoxO acetylation. We show that FoxO and its downstream regulation of c-Myc are tightly controlled through two independent and highly specific pathways of

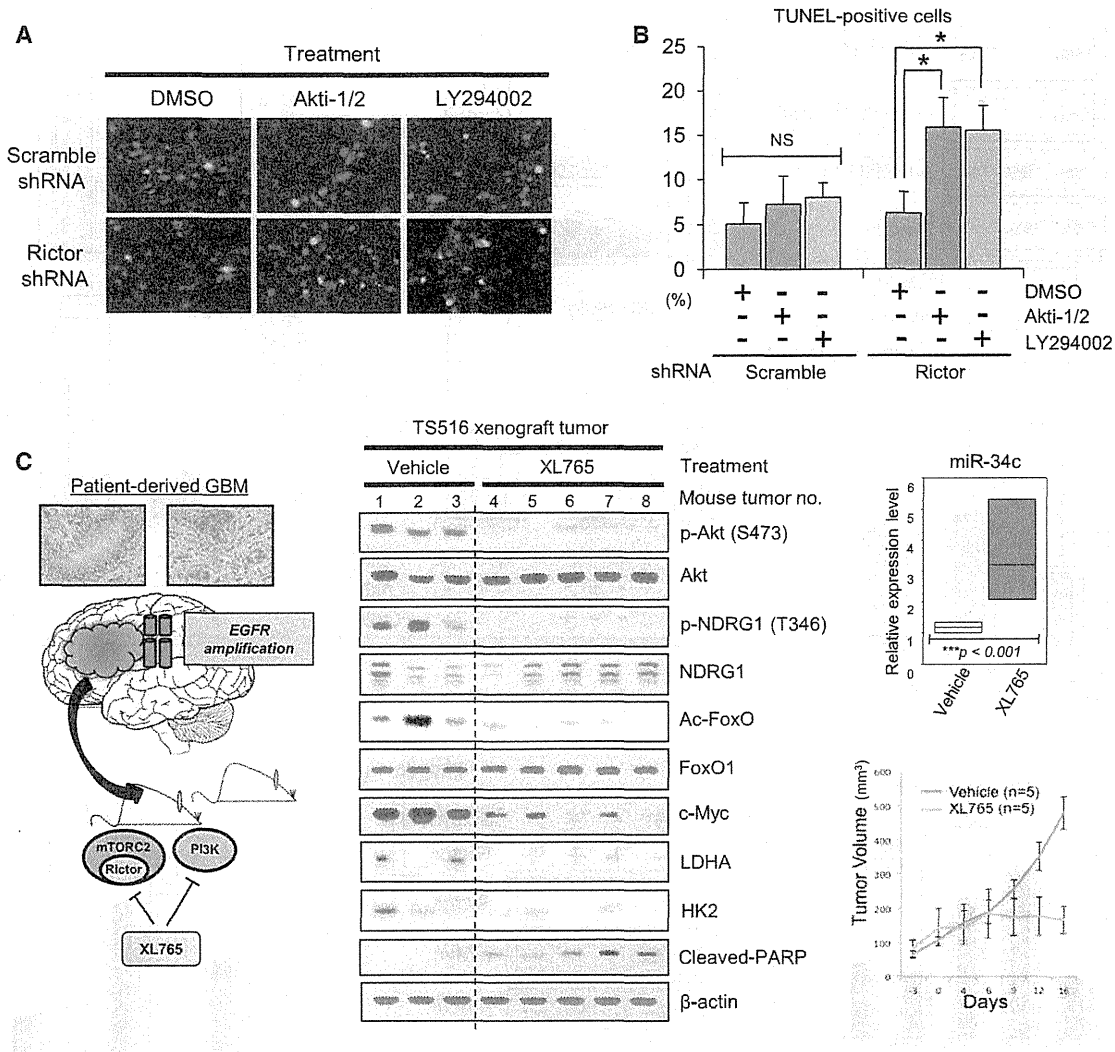

Figure 6. Combined Inhibition of PI3K/Akt and mTORC2 Suppresses Acetylated FoxO-Myc Signaling and Promotes Tumor Cell Death

(A) TUNEL staining in U87-EGFRvIII cells treated by PI3K/Akt inhibitors for 24 hr, combined with or without Rictor KD. Green, TUNEL staining; blue, DAPI staining.

(B) Quantified TUNEL-positive U87-EGFRvIII cells treated by PI3K/Akt inhibitors, combined with or without Rictor KD in the bar graph.

(C) An EGFR-amplified patient-derived TS516 GBM tumor sphere was implanted into immunodeficient mice that were subsequently treated with the dual PI3K/mTOR inhibitor XL765. Representative immunoblots displaying the status of FoxO acetylation, c-Myc and glycolytic enzyme expression, and apoptotic tumor cell death (cleaved PARP). Relative expression of miR-34c is shown in the box graph. Tumor volumes were measured by using length and width for vehicle-treated (n = 5) and XL765-treated (n = 5) groups.

Error bars, SEM.

posttranslational modification and microRNA suppression. One pathway, inactivating phosphorylation of FoxO by Akt, is a well-characterized mechanism enabling PI3K-activated tumor cells to engage c-Myc (Biggs et al., 1999; Bouchard et al., 2004; Delpuech et al., 2007; Dang, 2012a; Peck et al., 2013) by relieving FoxO-dependent miR-145 suppression of c-Myc. (Gan et al., 2010). In contrast, the results shown here identify a central mechanism of regulation of the FoxO-Myc axis to control glycolysis, as we demonstrate that mTORC2 controls the acetylation of FoxO through class IIa HDACs, independent of Akt.

The pathway identified here complements the previously demonstrated ability of mTORC2 to regulate glycolysis in the liver and in cancer cells through Akt activation (Dang, 2012b; Hagiwara et al., 2012; Plas and Thompson, 2005), providing yet another important signaling mechanism by which growth factor receptor mutations and tumor suppressor losses promote the Warburg effect in cancer (Bensaad et al., 2006; Christofk et al., 2008; Dang, 2012b; Faubert et al., 2013; Tong et al., 2009; Vander Heiden et al., 2009; Ward and Thompson, 2012). Thus, mTORC2 emerges as a particularly critical regulator of cancer cell metabolism through two mechanisms: Akt-dependent and Akt-independent signaling, each one regulating cellular levels of c-Myc by distinct posttranslational modifications of FoxO to relieve suppression of c-Myc through distinct suppressive microRNA networks. FoxO is a key intermediate between growth factor receptor PI3K signaling and c-Myc; thus, it is not surprising that the FoxO-Myc axis (Biggs et al., 1999; Bouchard et al., 2004; Delpuech et al., 2007; Dang, 2012a; Peck et al.,

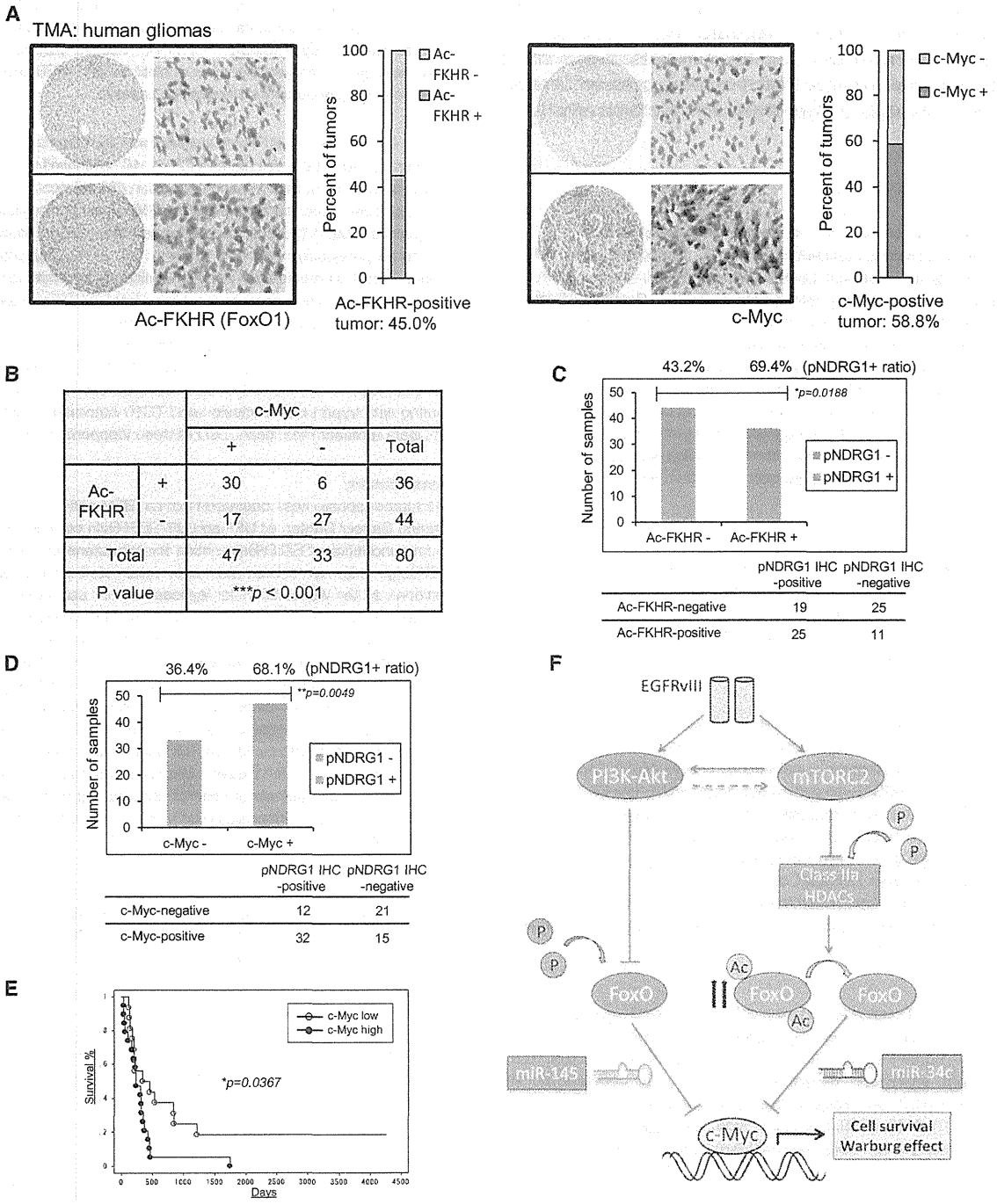

		c-Myc		
		+	-	Total
Ac-FKHR	+	30	6	36
	-	17	27	44
Total		47	33	80
P value		***$p < 0.001$		

Figure 7. mTORC2 Signaling, Acetylated FoxO, and c-Myc Expression Are Highly Intercorrelated in Biopsy Samples and Associated with Poor Prognosis in GBM Patients

(A) Ac-FoxO and c-Myc immunostaining of GBM tissue microarray (TMA) comprising 80 GBM samples and 26 normal brain tissue samples. View of the TMA slide and an example of a negative core and a positive core at high magnification to show cytoplasmic staining of Ac-FoxO and cytoplasmic/nuclear staining of c-Myc. Ac-FoxO and c-Myc are both individually upregulated in 45.0% and 58.8% of tumors, respectively.

(B) Immunohistochemical analysis of TMAs based on correlation of Ac-FoxO with c-Myc.

(C) Bar graph showing differential association of Ac-FoxO-positive or -negative tumors with p-NDRG1 IHC positivity based on TMA.

(D) Differential association of c-Myc ± tumors with p-NDRG1 immunopositivity based on TMA. p value was determined by χ^2 for independence test (B–D).

(E) Kaplan-Meier survival analysis for overall survival of 36 primary and secondary GBM samples classified by c-Myc expression. Log rank (Mantel-Cox) test was used to determine p values for Kaplan-Meier survival curve analyses.

(F) mTORC2 inhibits FoxO activity via acetylation, which could bypass PI3K/Akt inhibition, leading to the upregulation of c-Myc, a key downstream effector of cell proliferation and tumor metabolism in GBM.

See also Figure S5.